Electronic Supplementary Material (ESI) for Journal of Materials Chemistry A.

Fundamental role of Fe-N-C active sites in CO_2-derived ultra-porous carbon electrode for inhibiting shuttle phenomena in Li-S batteries

Jeongwoo Yang[a], Dong Woo Kang[a], Hodong Kim[a], Jae Hyun Park[a], Won Yeong Choi[a] and Jae W. Lee*[a]

[a]Department of Chemical and Biomolecular Engineering Korea Advanced Institute of Science and Technology (KAIST) Daejeon 34141, Republic of Korea

*Corresponding author. Tel: +82-42-350-3940. E-mail: jaewlee@kaist.ac.kr (Jae W. Lee)

KEYWORDS: CO_2 conversion, Ultrahigh porous carbon, Fe-N-C catalyst, Ammonia solution bubbling treatment, DFT calculations.

1. Experimental method

1. 1 Impregnation of sulfur

Carbon disulfide (CS_2, Sigma-Aldric, > 99%) and sulfur powder (Junsei, > 98%) were put in a glass vial and sonicated for 10 minutes to completely dissolve sulfur. TCPC/Fe-N-C powder was then added to the CS_2 solution in which sulfur was dissolved (mass ratio of sulfur:TCPC/Fe-N-C = 3:2). For the fabrication of a high loading electrode, the sulfur content was set to 80 wt% (mass ratio of sulfur:TCPC/Fe-N-C = 4:1). The as-prepared powder was heated to 155 °C (at 5 °C min^{-1}) and held in an Ar atmosphere for 12 hours. CPC and UCPC/Fe-N-C were impregnated with sulfur by the same procedure as employed for TCPC/Fe-N-C.

1. 2 Synthesis of Li_2S_6 and Li_2S_8 catholyte

The sulfur and Li_2S (Sigma-Aldrich, 99.98%) at a molar ratio of 5:1 were added to a mixture of DME (dimethyl ether, Sigma-Aldrich, > 99%) and DOL (1,3-dioxolane, Sigma-Aldrich, 99.8%) (volume ratio of DME:DOL = 1:1) and stirred at 60 °C for 24 hours in a glove box filled with Ar for fabrication of Li_2S_6. The final concentration was adjusted to 0.5 M of Li_2S_6 in the DME and DOL solution. To prepare the Li_2S_6 solution for a symmetric cell, sulfur (S_8) and Li_2S were added to a mixture of DME and DOL (volume ratio of DME:DOL 1:1) in which 1 M of LiTFSi (Lithium bis(trifluoromethanesulfonyl)imide, Sigma-Aldrich, 99.95%) was dissolved. Li_2S_8 catholyte was additionally prepared for Li_2S nucleation test. The molar ratio of sulfur and Li_2S was set to 7:1, and the other conditions were the same as for the Li_2S_6 catholyte.

1. 3 Fabrication of symmetric cells and evaluation of catalytic effect of Fe-N-C

TCPC/Fe-N-C and PVDF (Sigma-Aldrich, average Mw 534000) with a weight ratio of 9:1

were mixed in NMP (Alfa Aesar, 99.5%) and stirred homogeneously for 24 hours. The well-mixed slurry was coated on carbon paper, which was dried at 60 °C for 12 hours. The TCPC/Fe-N-C coated paper was punched into a circular shape with a size of 1 cm in diameter. CPC and UCPC/Fe-N-C electrodes were prepared in the same manner. Two TCPC/Fe-N-C electrodes were fabricated in a symmetric battery with each electrode side contained 0.5 M Li2S6 electrolyte. Cyclic voltammetry (CV) was carried out at a scan rate of 10 mV s^{-1} in a voltage range of −1.0-1.0 V at room temperature with a WonATech battery test system. For the nucleation test, the ratio of the coated active material was set to 0.8-1.0 mg cm^{-2}. For the cell assembly, 10 uL of the conventional electrolyte in which lithium sulfide species were not dissolved was placed on the Li foil anode region, and 10 uL of prepared Li_2S_8 electrolyte was dropped on the cathode region.

1.4 Electrochemical measurements

First, a slurry for the sulfur electrode was prepared by mixing TCPC/Fe-N-C/S, carbon black (Alfa Aesar, > 99%), and PVDF with a mass ratio of 8:1:1 in NMP. The slurry was stirred with a magnetic bar for 24 hours. After stirring, it was casted on Al foil. The casted foil was dried at 60 °C for 12 hours, and then the sulfur electrode was punched into a circular shape with a diameter of 1 cm. In the case of other materials, the electrodes were manufactured in the same manner as above. The areal sulfur loading amount on each electrode was adjusted to 1.4 mg cm^{-2}. 1 M LiTFSI dissolved in DME and DOL with 0.2 M $LiNO_3$ (Sigma-Aldrich, 99.99%) additive was used as the electrolyte. In the case of the standard electrode, the electrolyte volume was 15 uL mg^{-1}, and the volume was 10 uL mg^{-1} for the high sulfur loading electrode. Lithium metal was used as the counter electrode. Celgard 2400 with a diameter of 1.4 cm was used as a separator. Finally, coin cell (2032-type) were assembled inside a glove box. CV was

performed in a range of 1.7−2.8 V and EIS was carried out in a range of frequency of 100 kHz to 10 mHz.

1.5 In-situ vial cell test and static adsorption test

CPC, TCPC/Fe-N-C electrodes, and Li metal were put into a vial containing the electrolyte and discharged for 10 hours at 0.1 C current density. The vial cell was prepared in a glove box, and the color change over time was identified by a digital camera. An adsorption test was performed by adding CPC and TCPC/Fe-N-C powder to the prepared Li_2S_6 solution. Visual changes were confirmed using a digital camera. After conducting the adsorption test for 12 hours, each solution was transferred into a quartz cell for UV–Vis measurement in a glove box, and the concentration of Li_2S_6 remaining in the solution was determined.

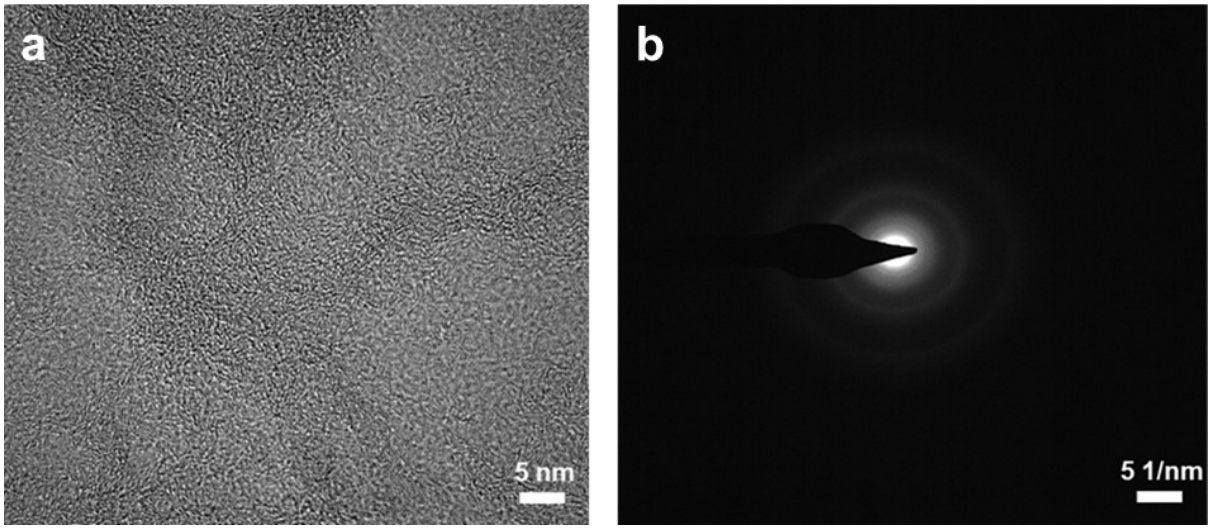

Fig. S1 a) High magnification TEM image, b) SAED pattern of CPC.

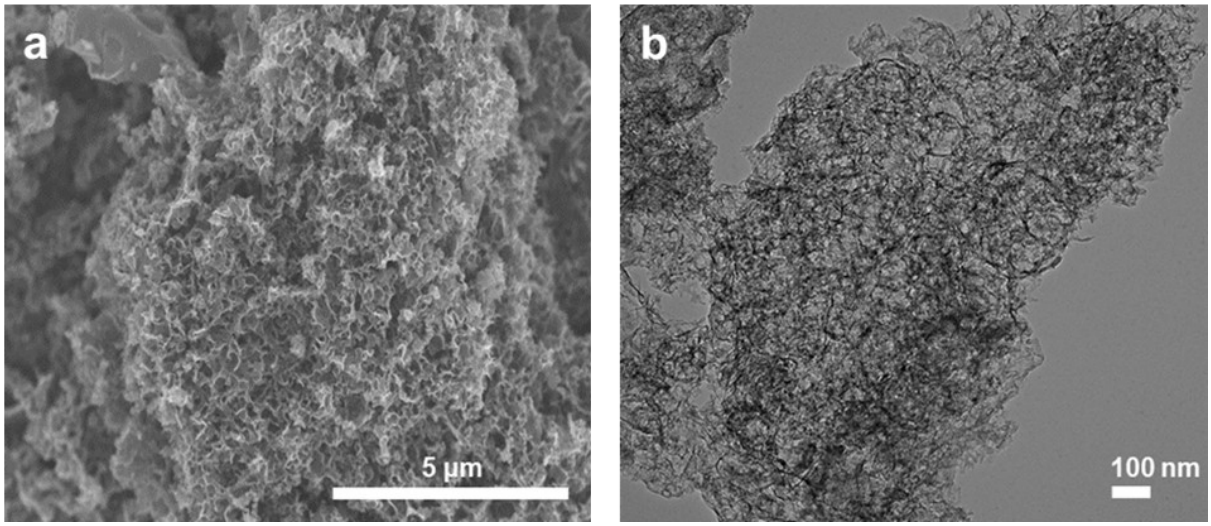

Fig. S2 a) SEM, b) TEM images of UCPC/Fe-N-C.

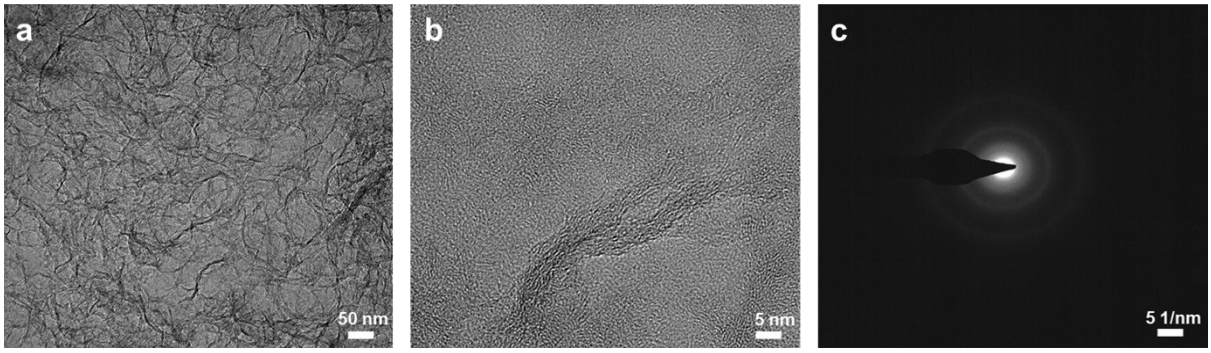

Fig. S3 a,b) High-resolution TEM images, c) SAED pattern of TCPC/Fe-N-C.

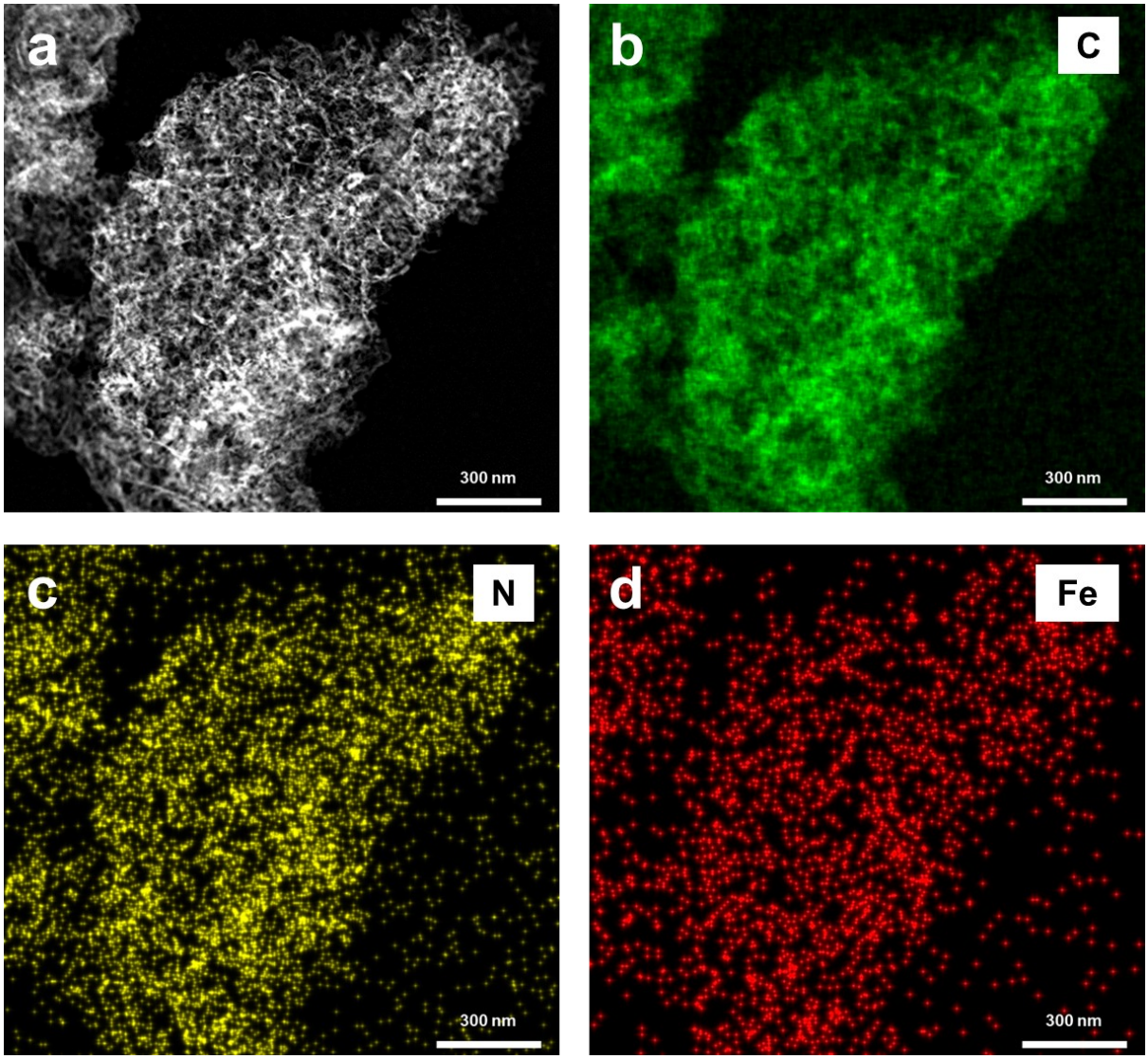

Fig. S4 a) Dark-field STEM image, and the corresponding b) C, c) N, and d) Fe elemental mapping images of UCPC/Fe-N-C.

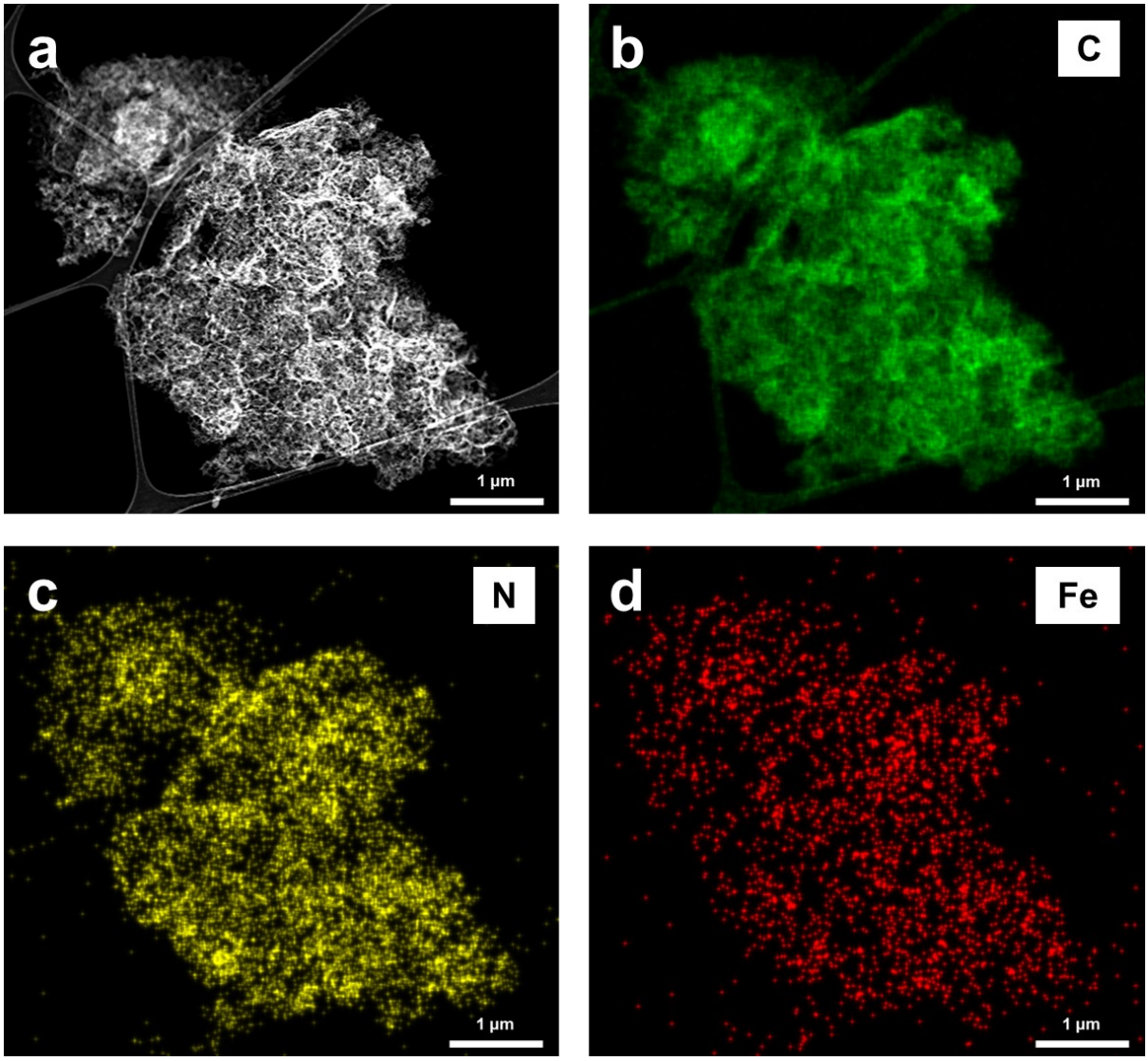

Fig. S5 a) Dark-field STEM image, and the corresponding b) C, c) N, and d) Fe elemental mapping images of TCPC/Fe-N-C.

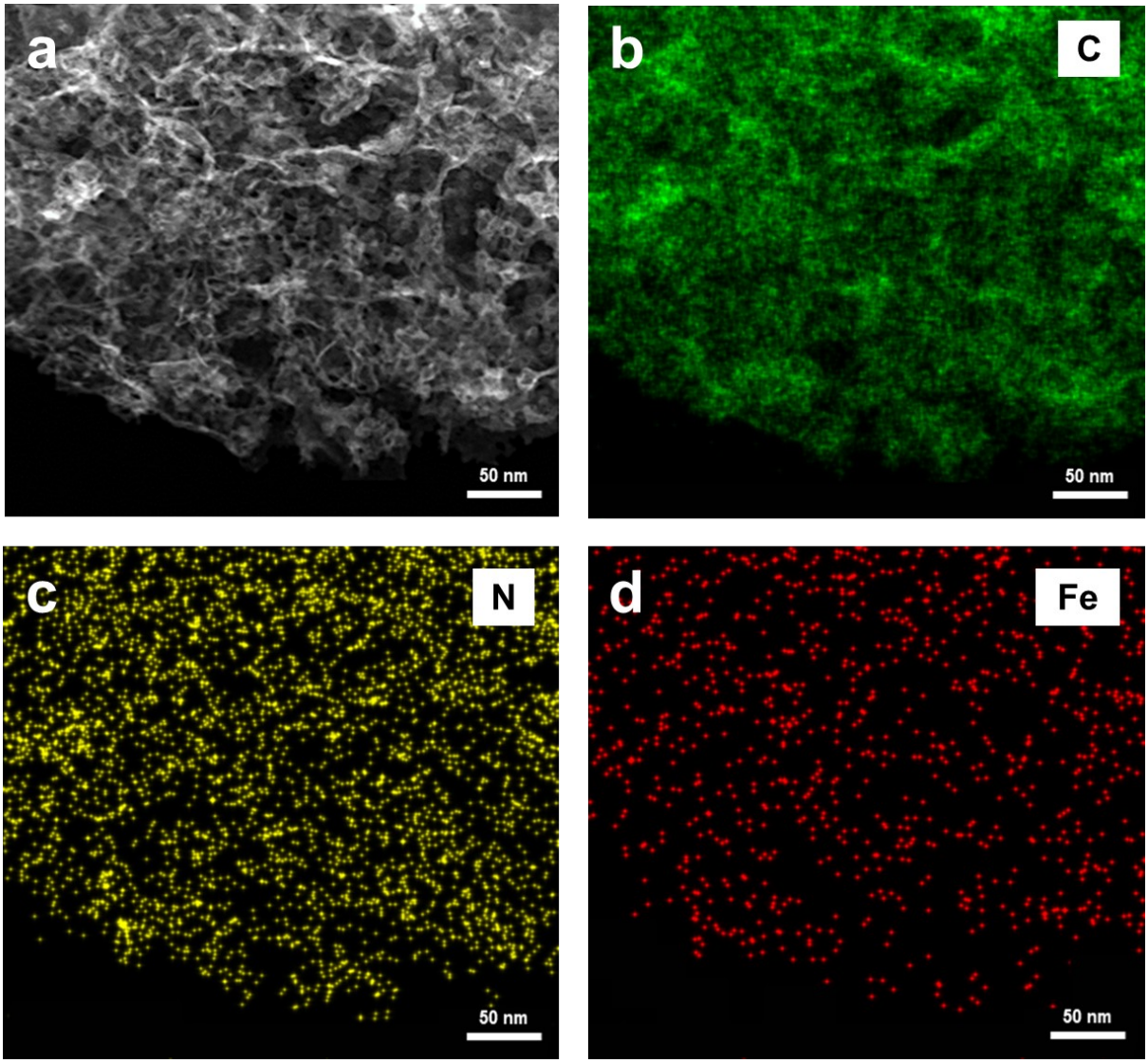

Fig. S6 a) High-resolution Dark-field STEM image, and the corresponding b) C, c) N, and d) Fe elemental mapping images of TCPC/Fe-N-C.

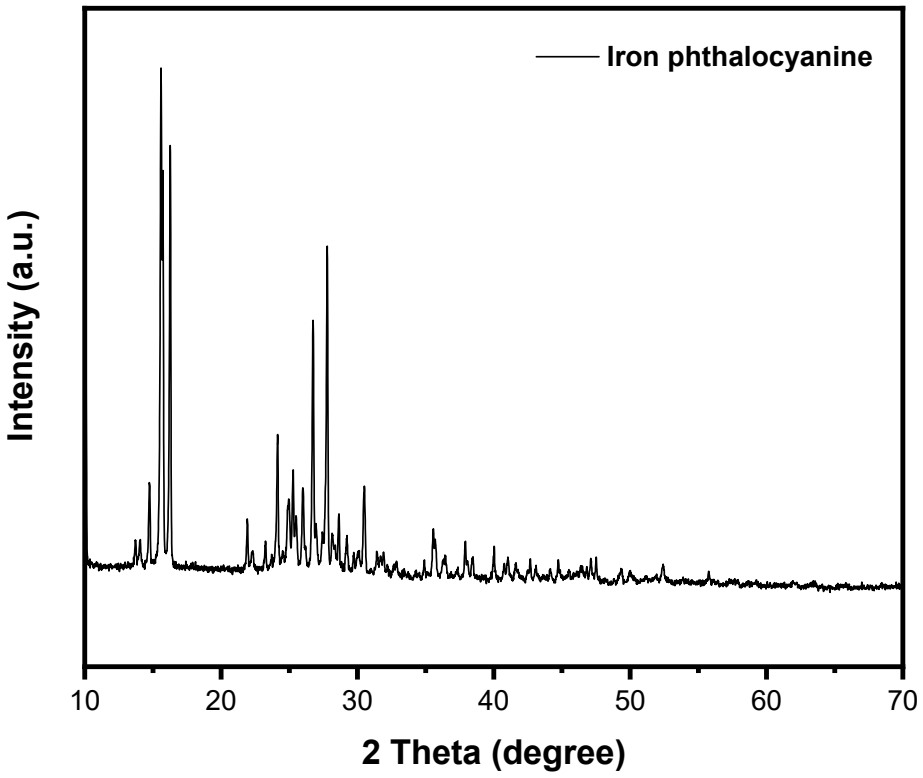

Fig. S7 XRD spectrum of FePC.

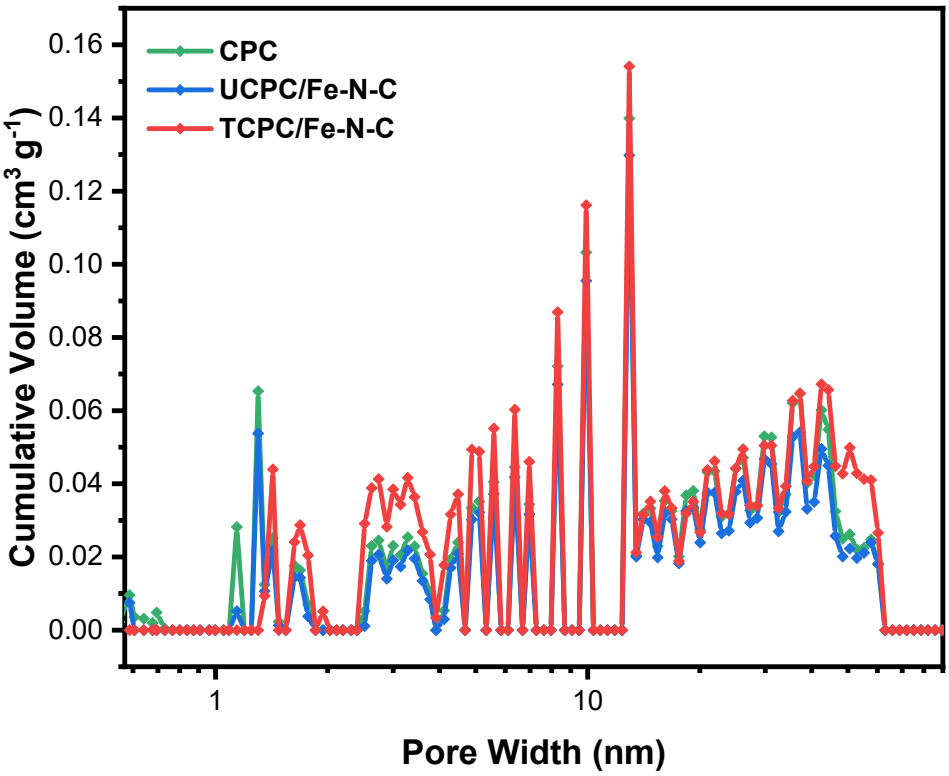

Fig. S8 NLDFT pore size distribution for CPC, UCPC/Fe-N-C, and TCPC/Fe-N-C.

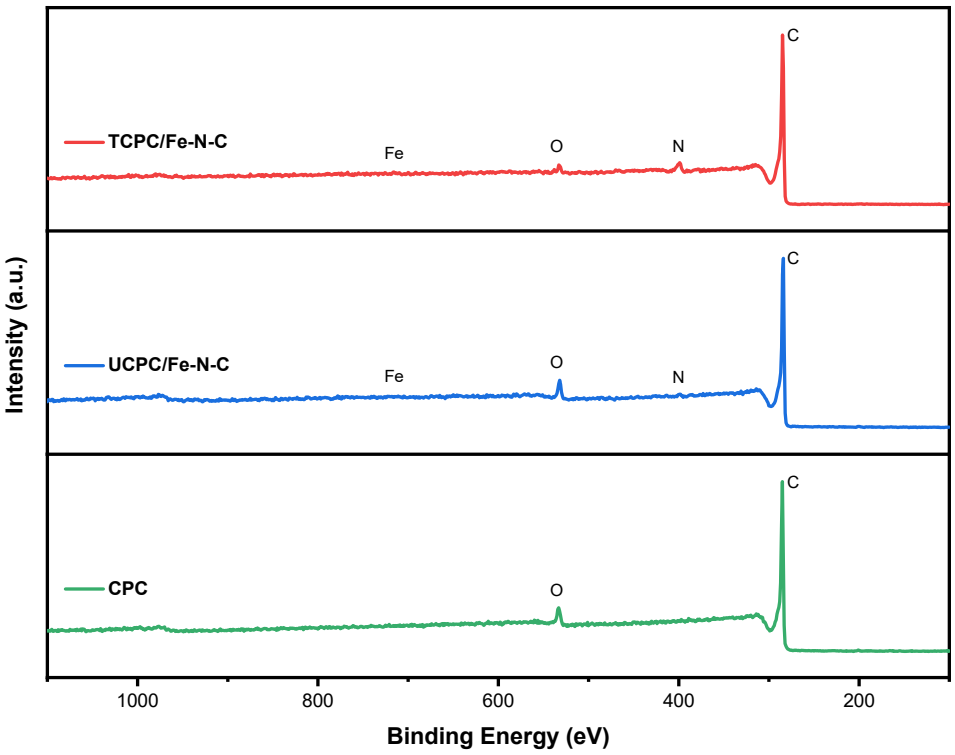

Fig. S9 XPS survey data of CPC, UCPC/Fe-N-C, and TCPC/Fe-N-C.

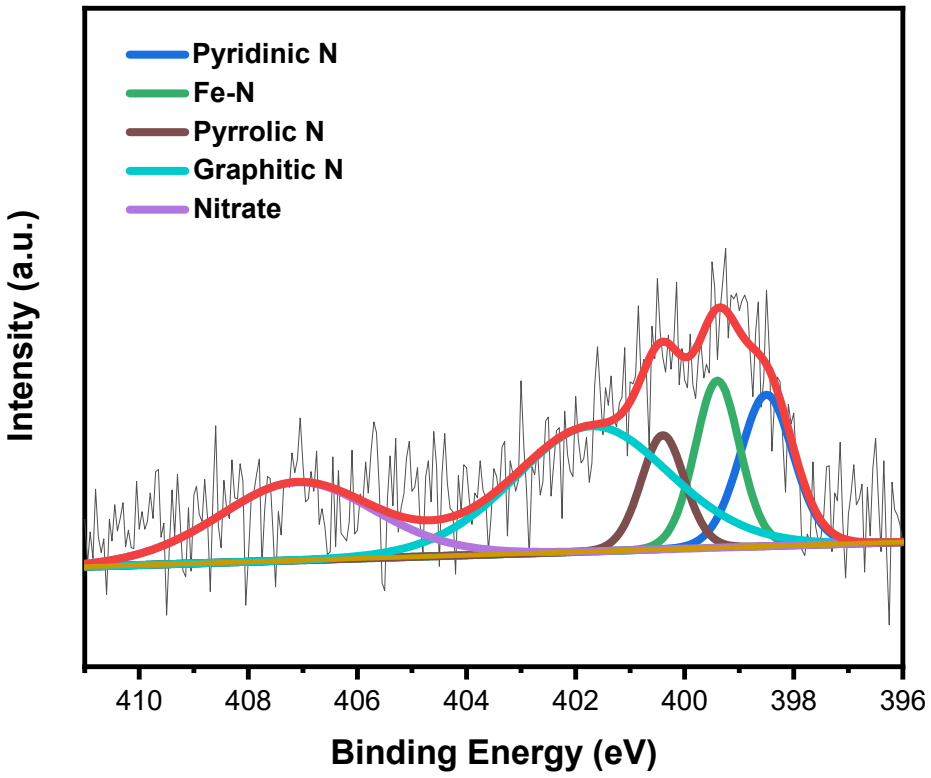

Fig. S10 XPS N 1s spectra of UCPC/Fe-N-C.

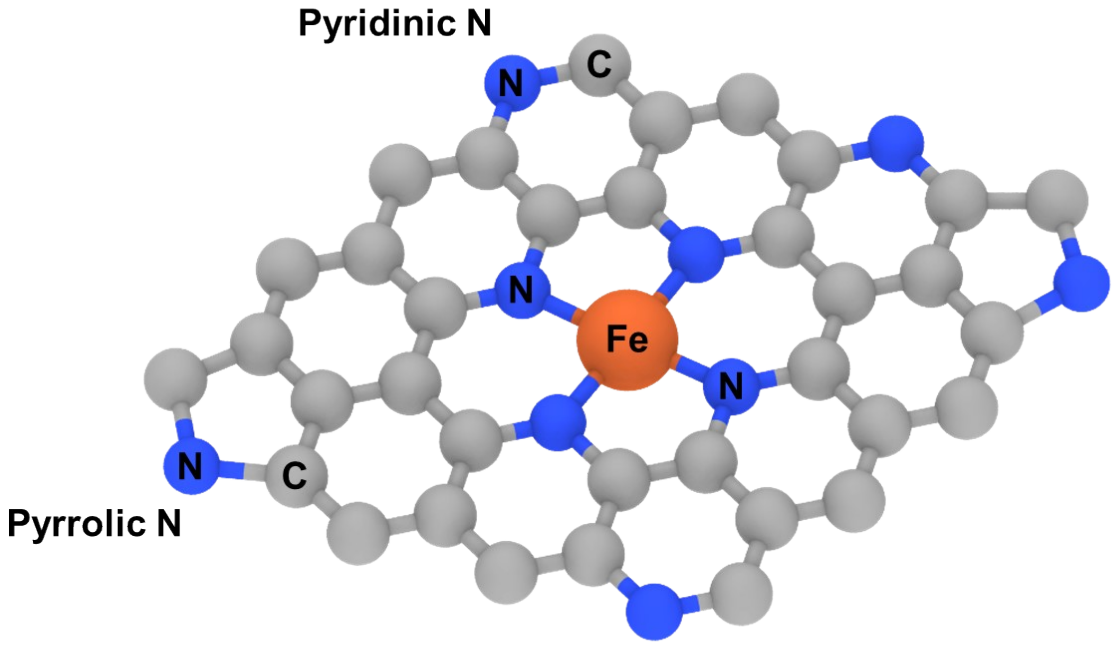

Fig. S11 The schematic image of nitrogen site.

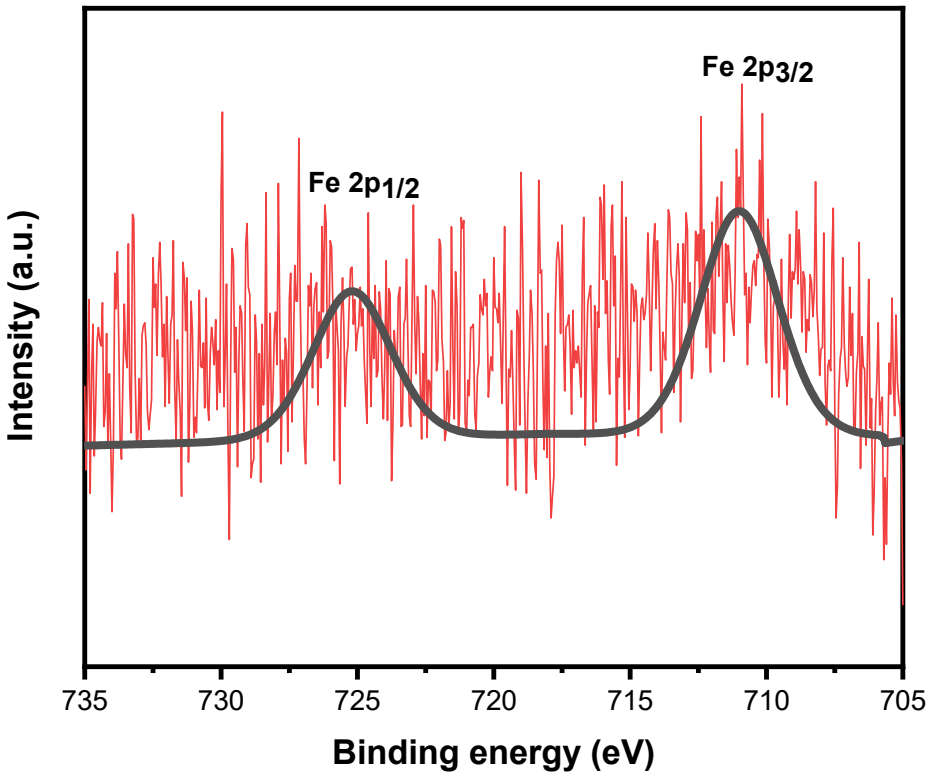

Fig. S12 XPS Fe 2p spectrum of TCPC/Fe-N-C.

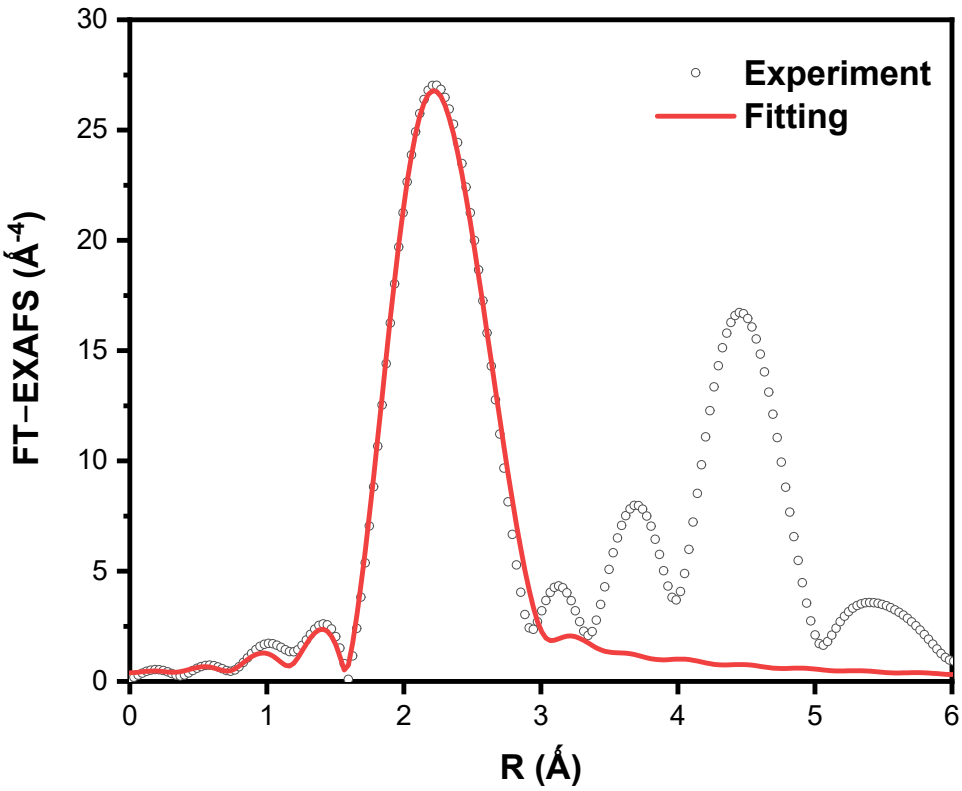

Fig. S13 EXAFS fitting curve of reference Fe foil.

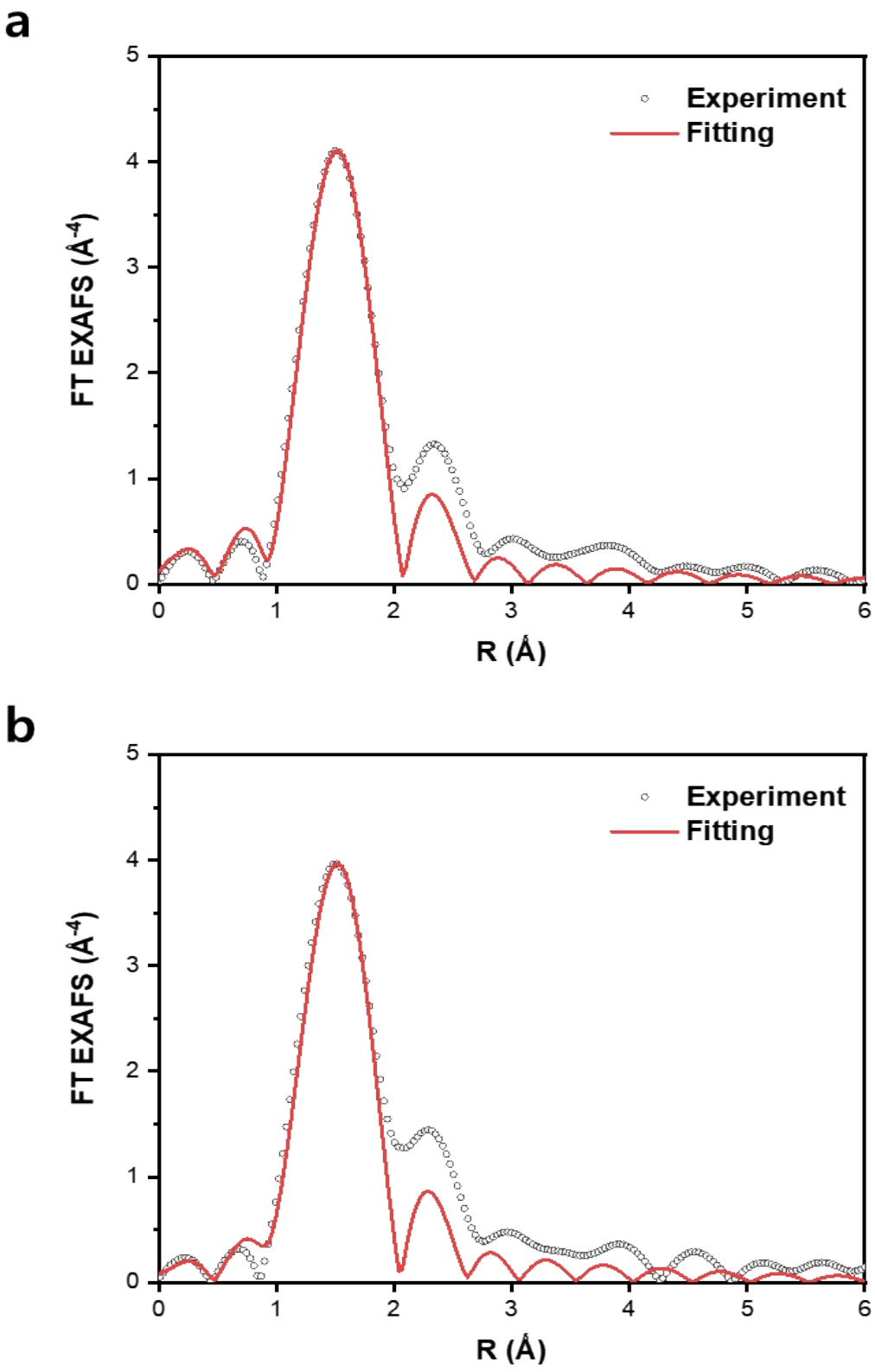

Fig. S14 EXAFS fitting curve of a) TCPC/Fe-N-C, b) UCPC/Fe-N-C.

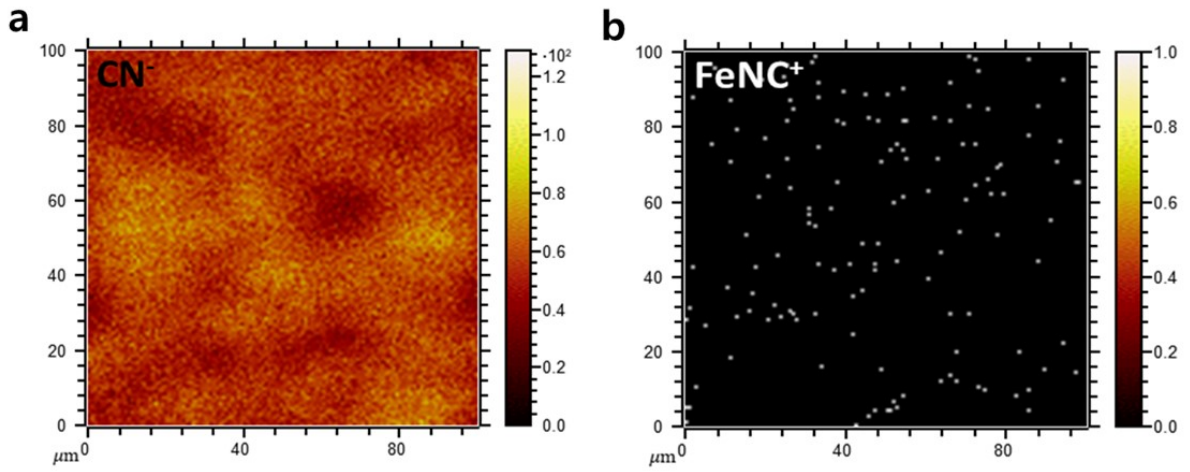

Fig. S15 ToF-SIMS CN^- negative ion image and $FeNC^+$ positive ion image of UCPC/Fe-N-C.

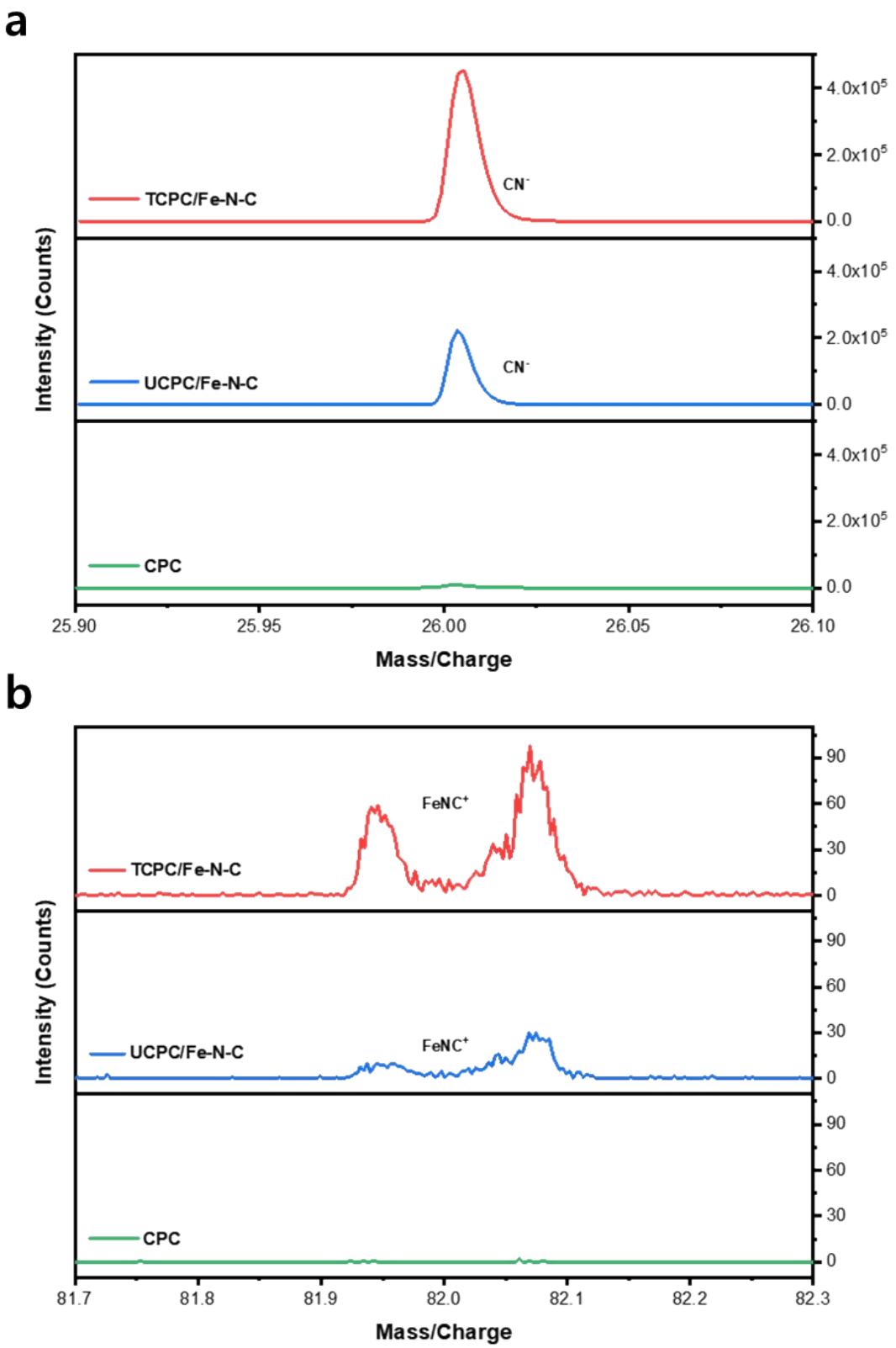

Fig. S16 ToF-SIMS ion spectra of a) negative ion of CN^-, b) postive ion of $FeNC^+$.

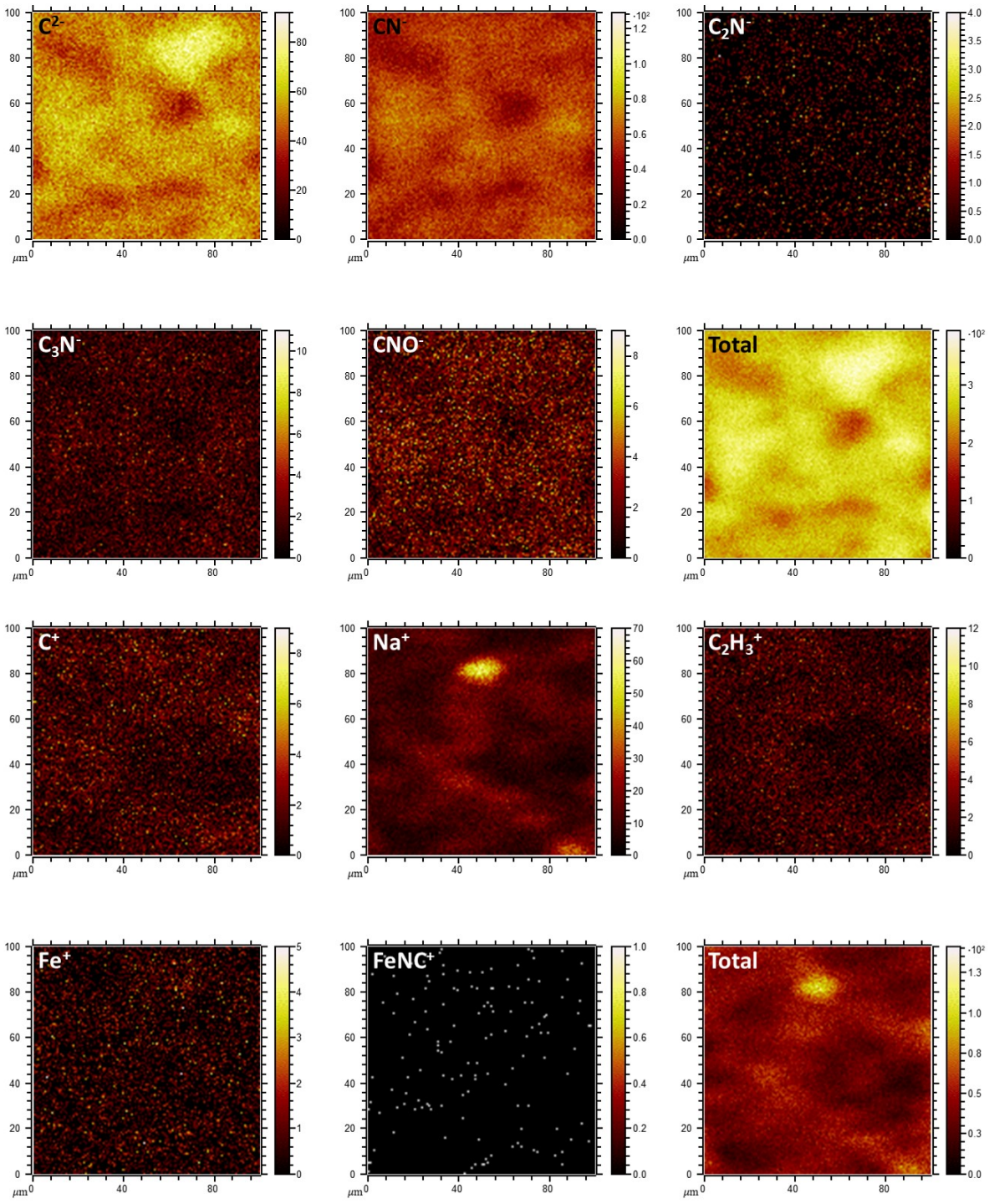

Fig. S17 ToF-SIMS negative and positive ion images of UCPC/Fe-N-C.

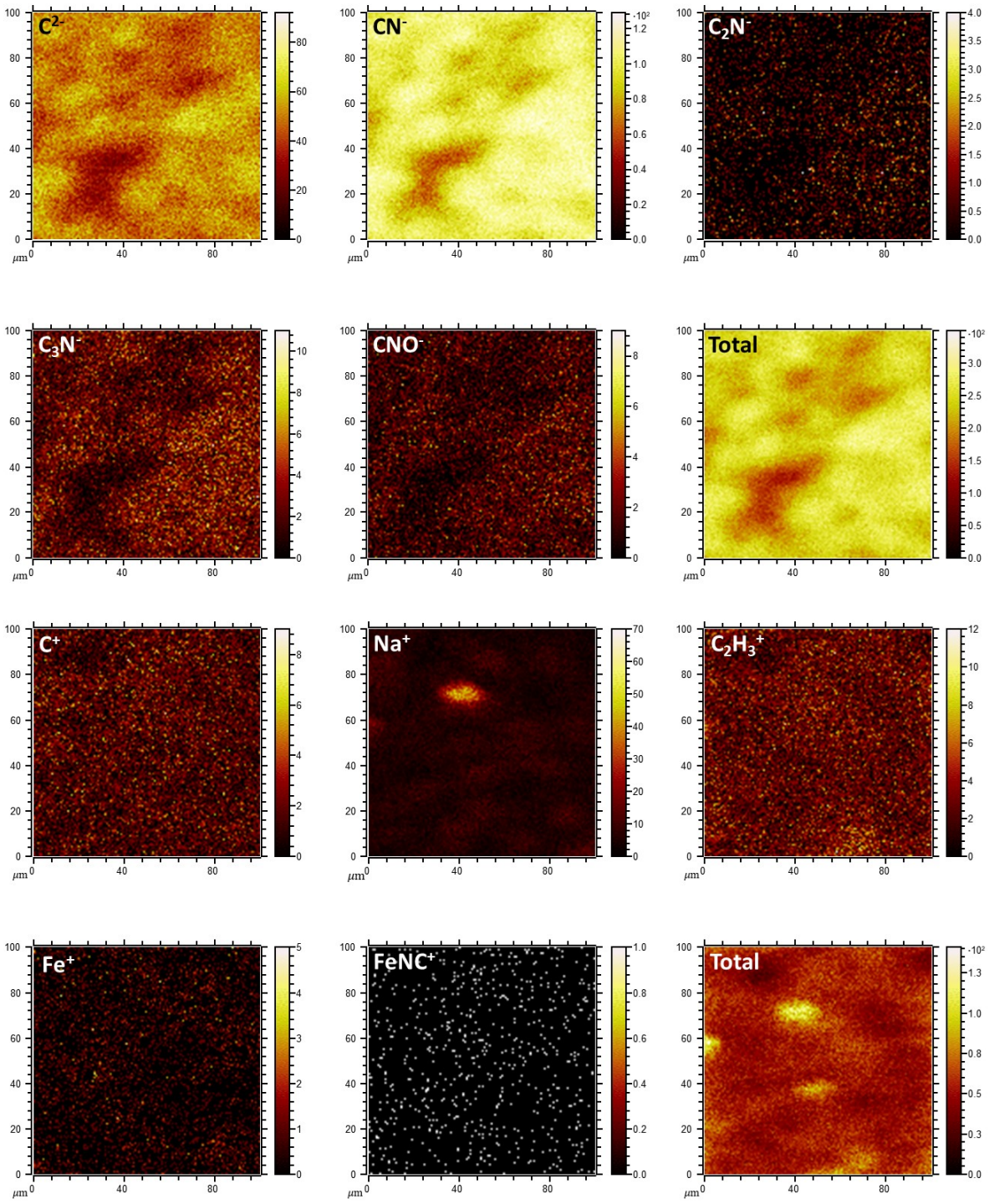

Fig. S18 ToF-SIMS negative and positive ion images of TCPC/Fe-N-C.

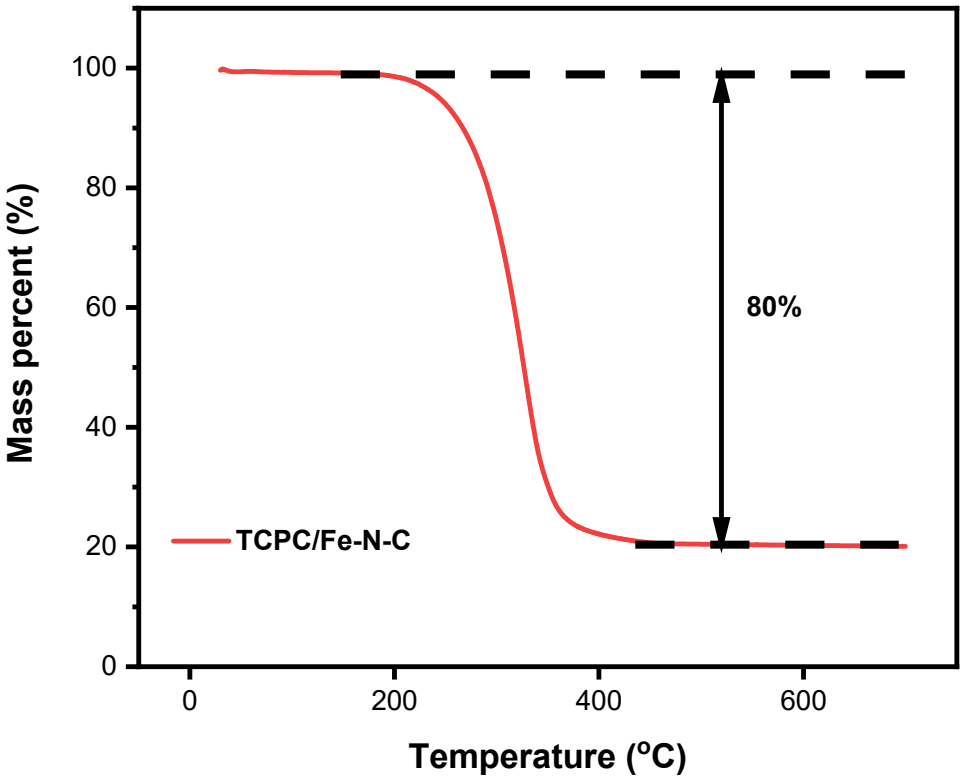

Fig. S19 TGA data for high sulfur loading electrode with TCPC/Fe-N-C.

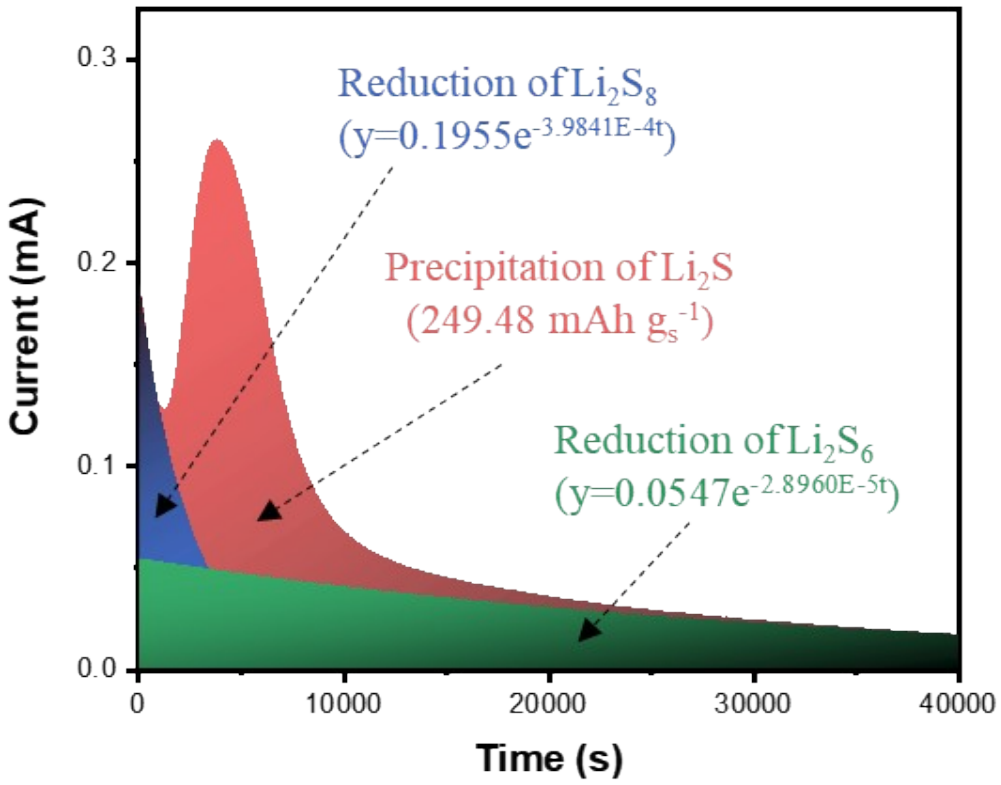

Fig. S20 Potentiostatic discharge curve of Li_2S nucleation process at 2.09 V for UCPC/Fe-N-C.

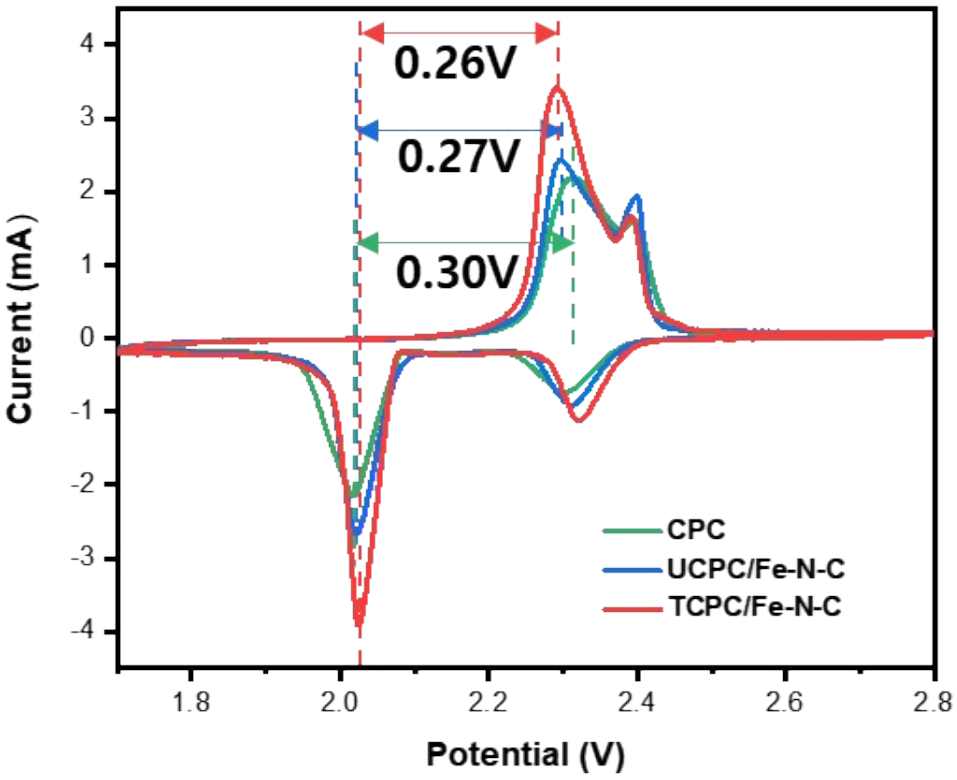

Fig. S21 The CV data of CPC, UCPC/Fe-N-C, and TCPC/Fe-N-C at 0.1 mV s^{-1} scan rate.

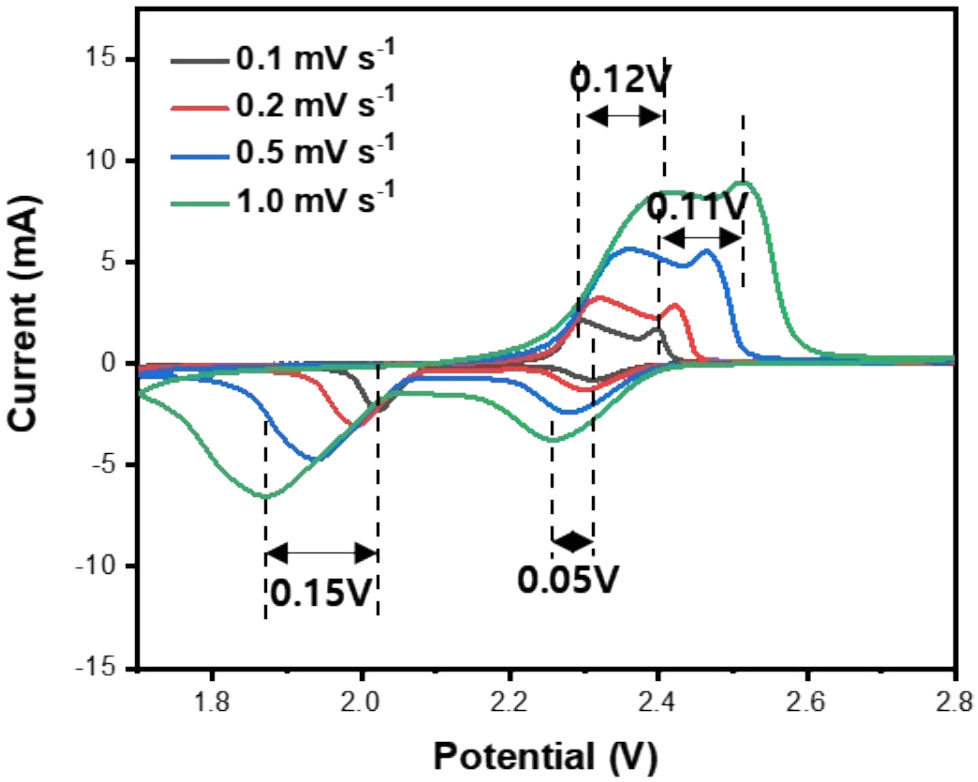

Fig. S22 The CV graph for UCPC/Fe-N-C

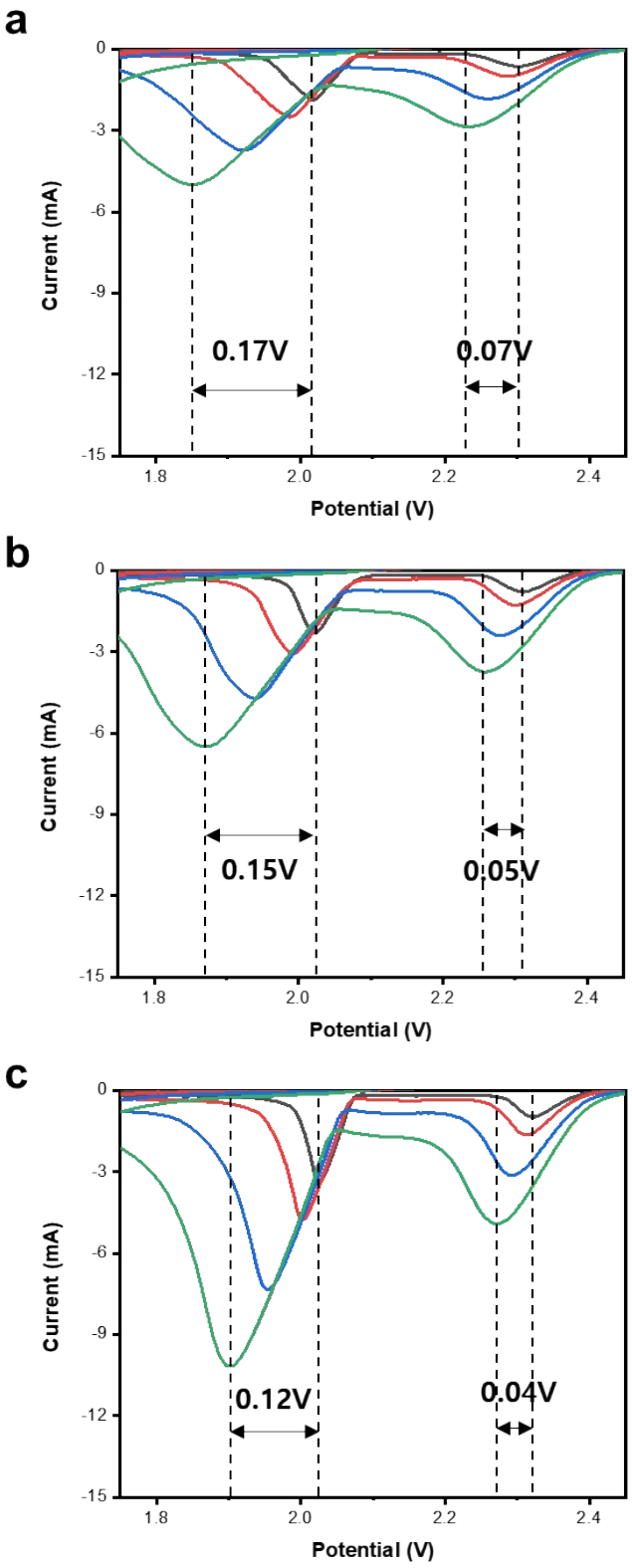

Fig. S23 The measured cathodic currents of a) CPC, b) UCPC/Fe-N-C, c) TCPC/Fe-N-C.

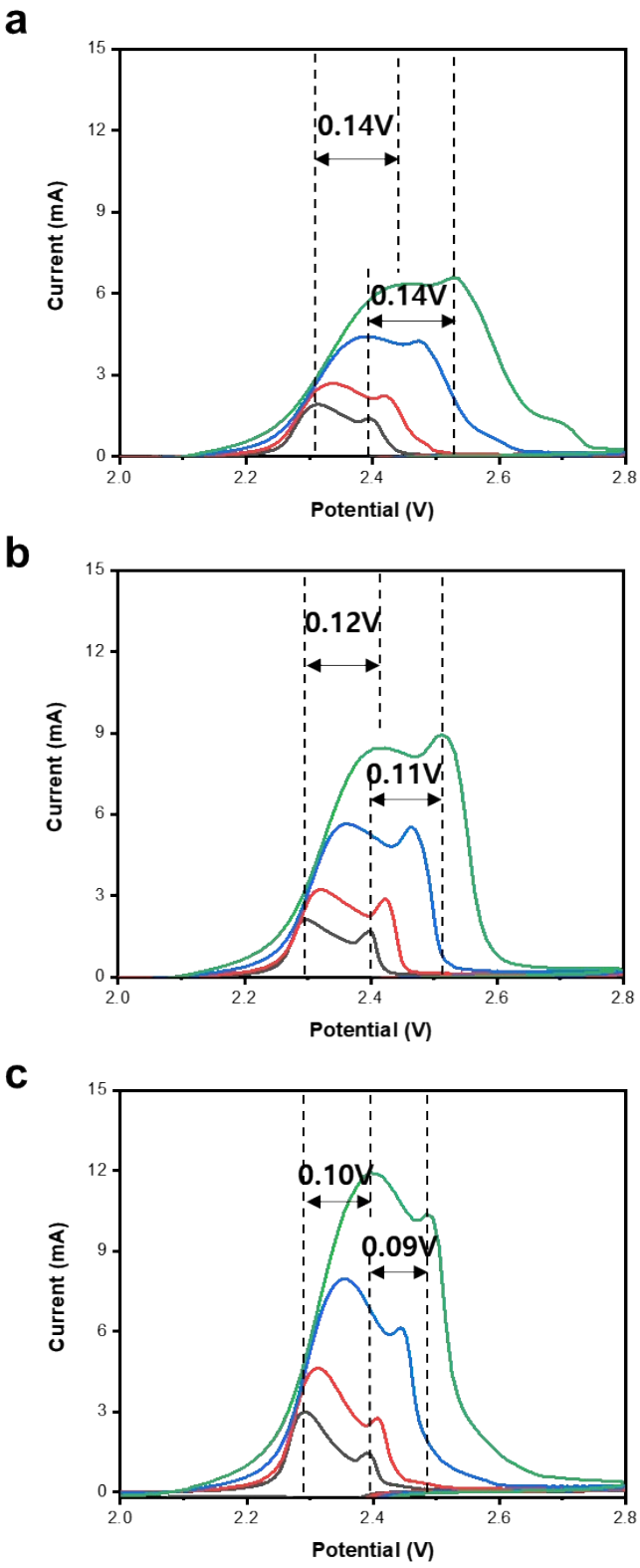

Fig. S24 The measured anodic currents of a) CPC, b) UCPC/Fe-N-C, c) TCPC/Fe-N-C.

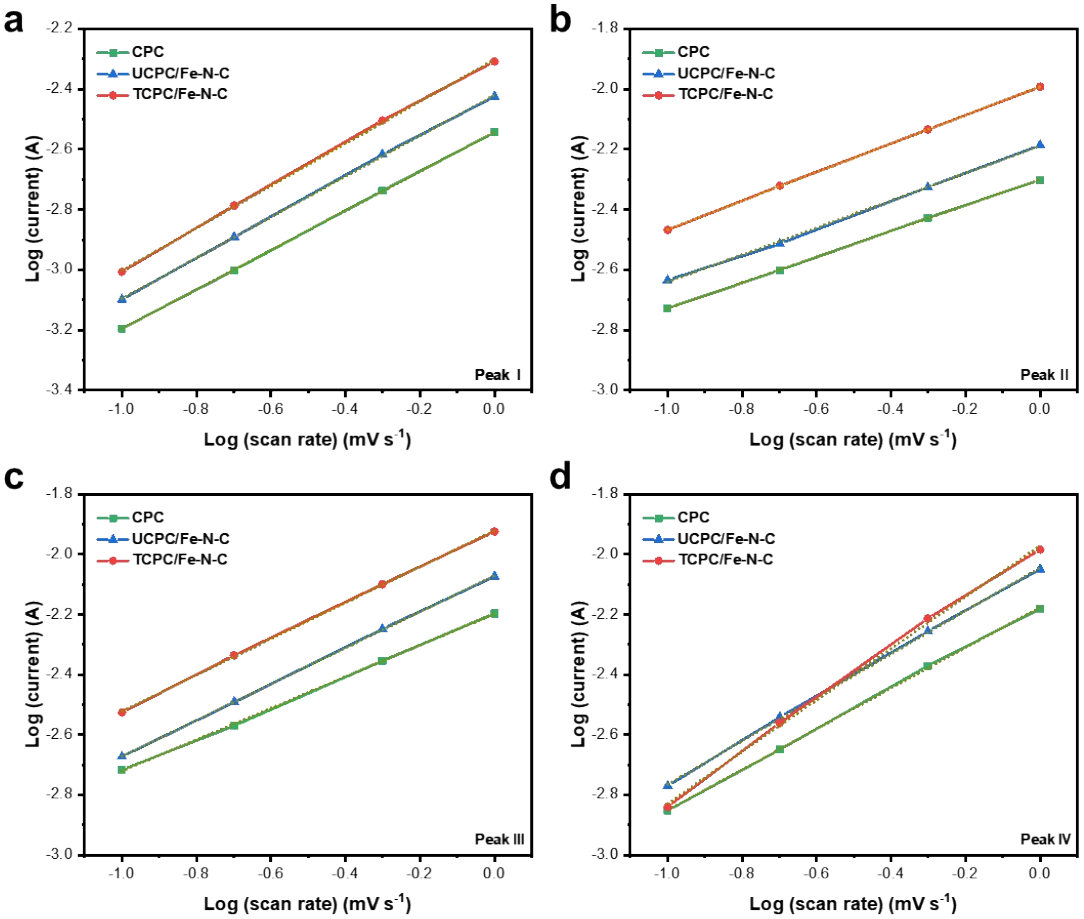

Fig. S25 Linear plots of logged current versus logged scan rate for four peaks with CPC, UC PC/Fe-N-C, and TCPC/Fe-N-C.

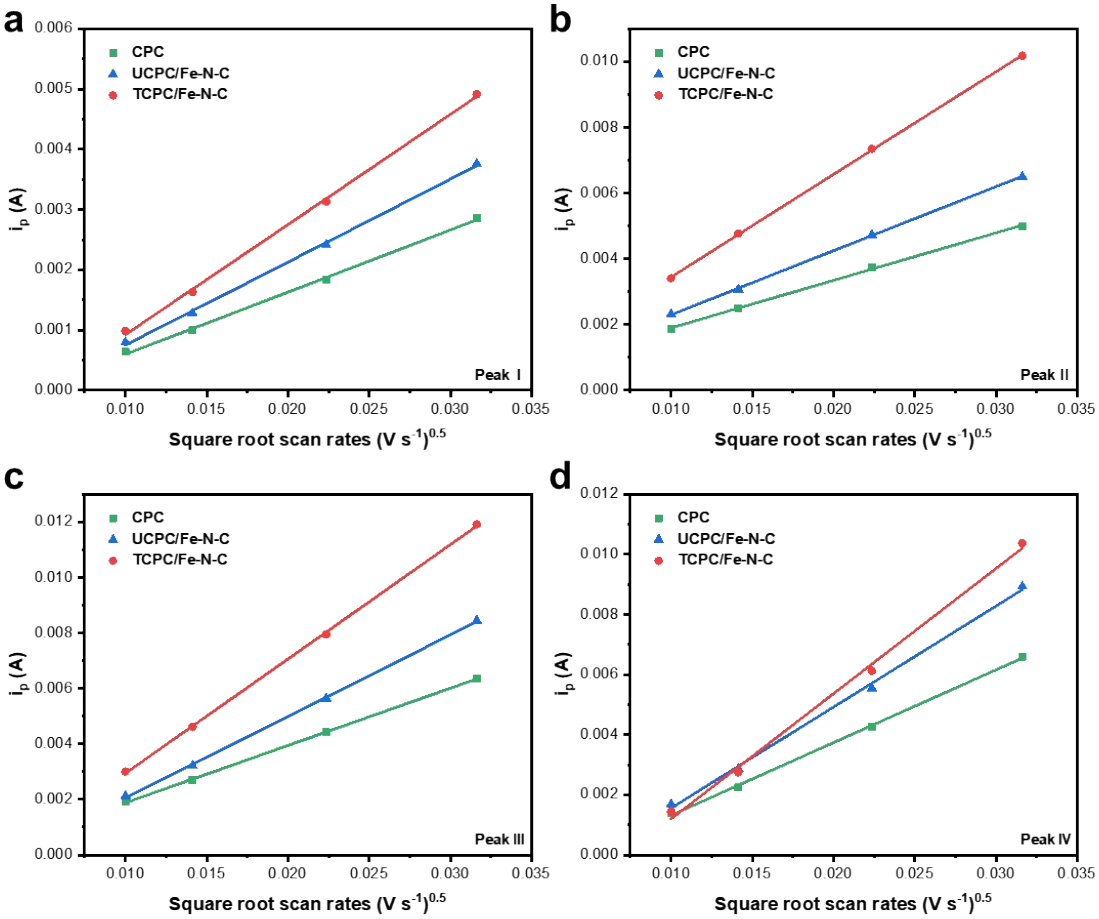

Fig. S26 Linear plots of CV peak current versus root of scan rate for four peaks with CPC, UCPC/Fe-N-C, and TCPC/Fe-N-C.

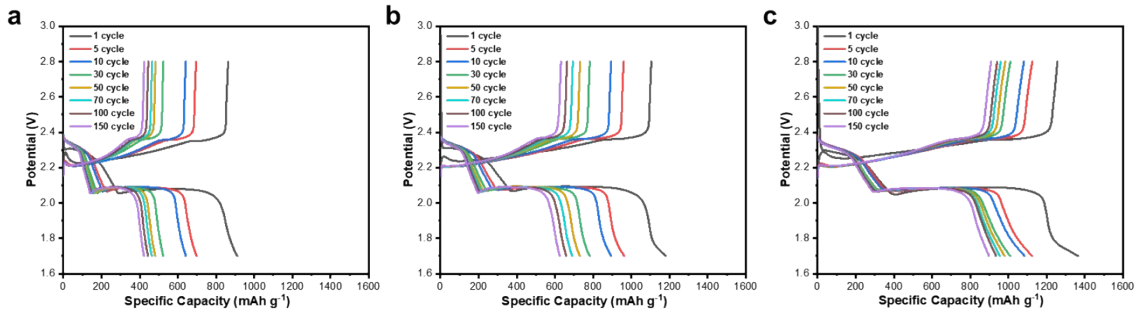

Fig. S27 Galvanostatic voltage profile graphs for a) CPC, b) UCPC/Fe-N-C, c) TCPC/Fe-N-C at 0.5 C.

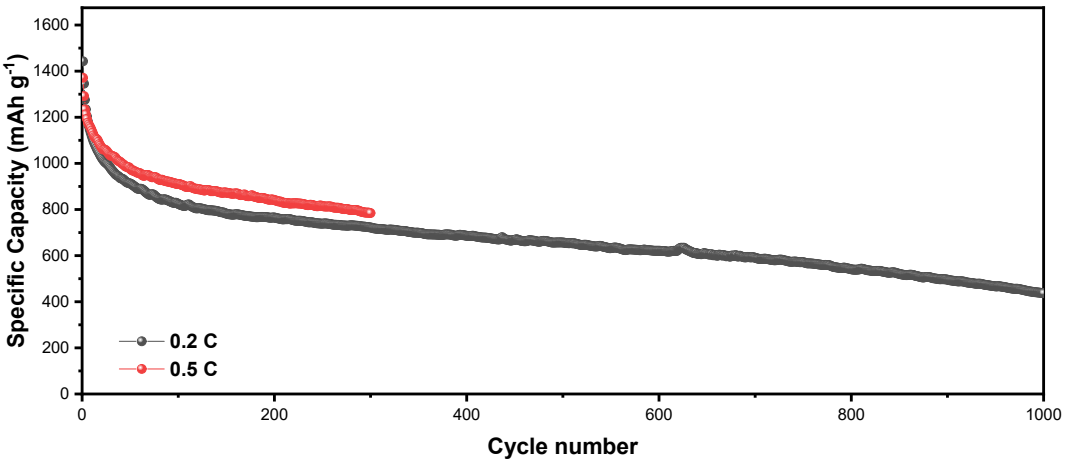

Fig. S28 Long cycle performance graph of TCPC/Fe-N-C at 0.2 and 0.5 C rate.

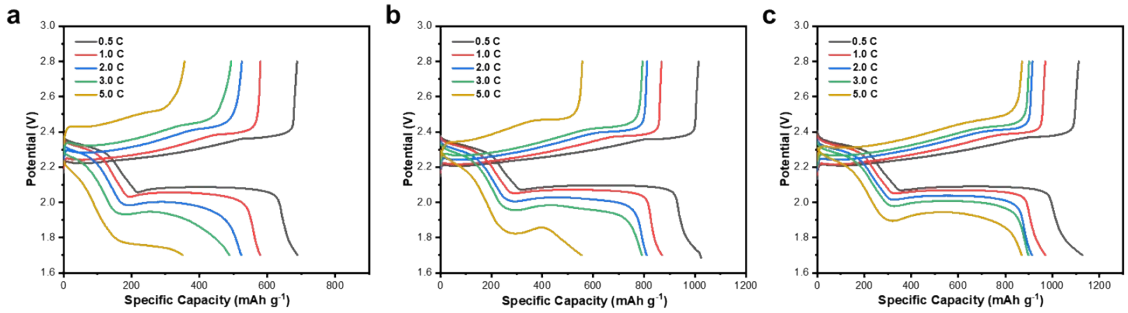

Fig. S29 Voltage profiles of a) CPC, b) UCPC/Fe-N-C, c) TCPC/Fe-N-C operated at different current densities.

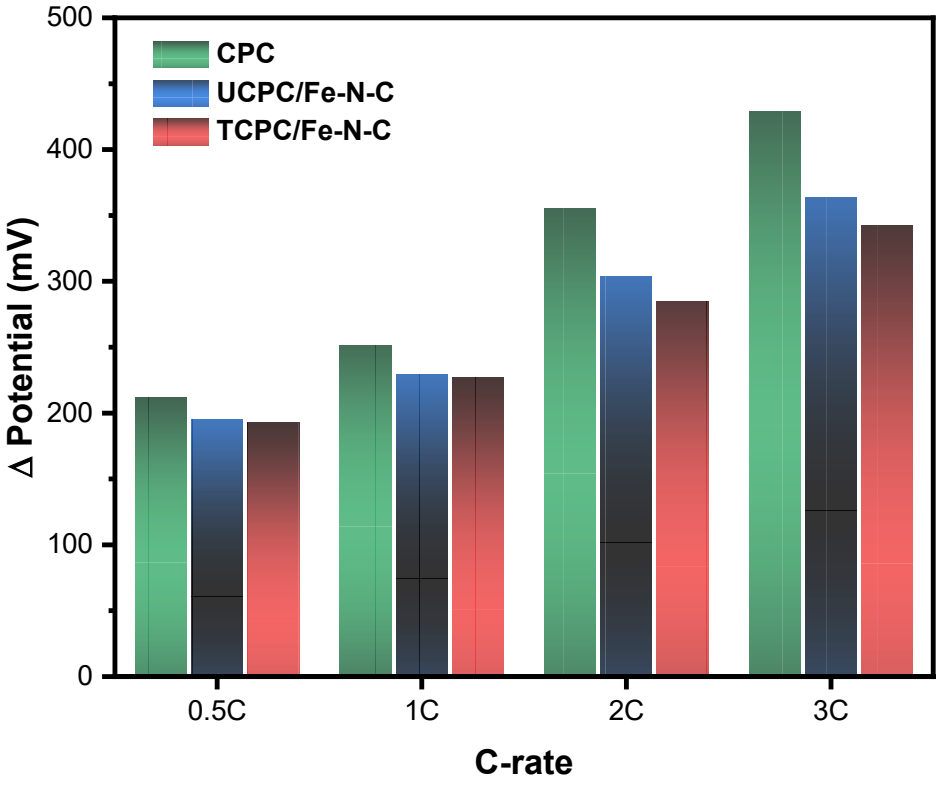

Fig. S30 Voltage gap of CPC, UCPC/Fe-N-C, and TCPC/Fe-N-C operated at different current densities.

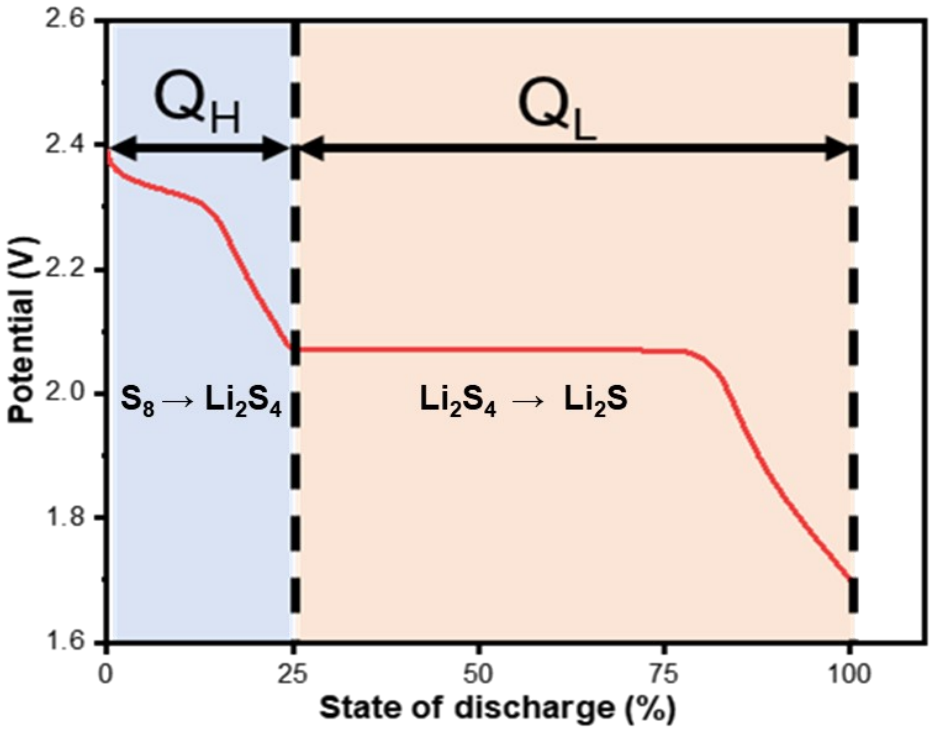

Fig. S31 Schematic of voltage profile curve during discharge process in Li-S batteries.

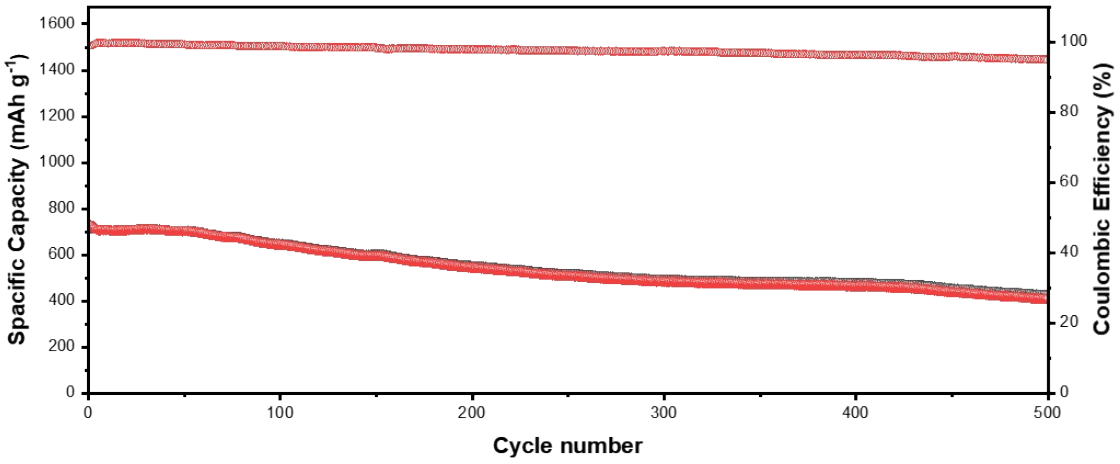

Fig. S32 The cycle performance of TCPC/Fe-N-C at 7.0 C rate.

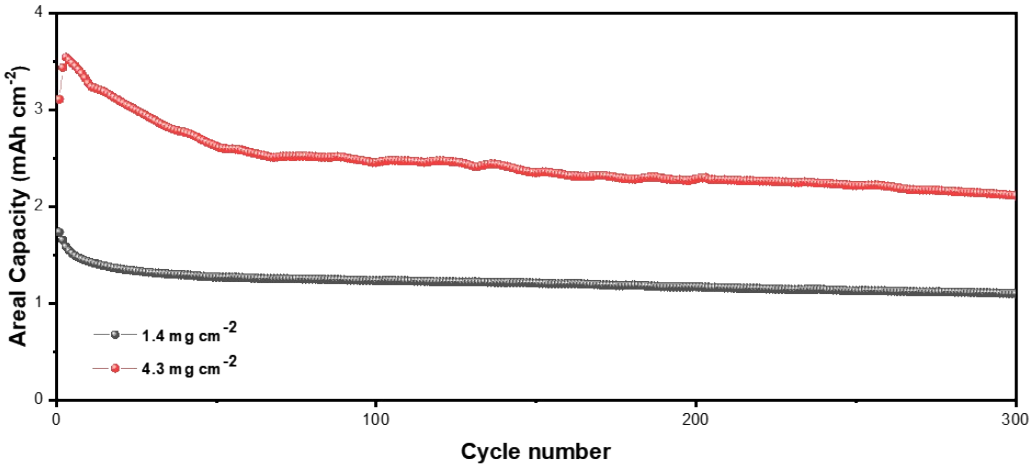

Fig. S33 The cycle performance for 1.4 mg cm^{-2} and 4.3 mg cm^{-2} with sulfur-loaded TCPC/Fe-N-C electrode at 1.0 C.

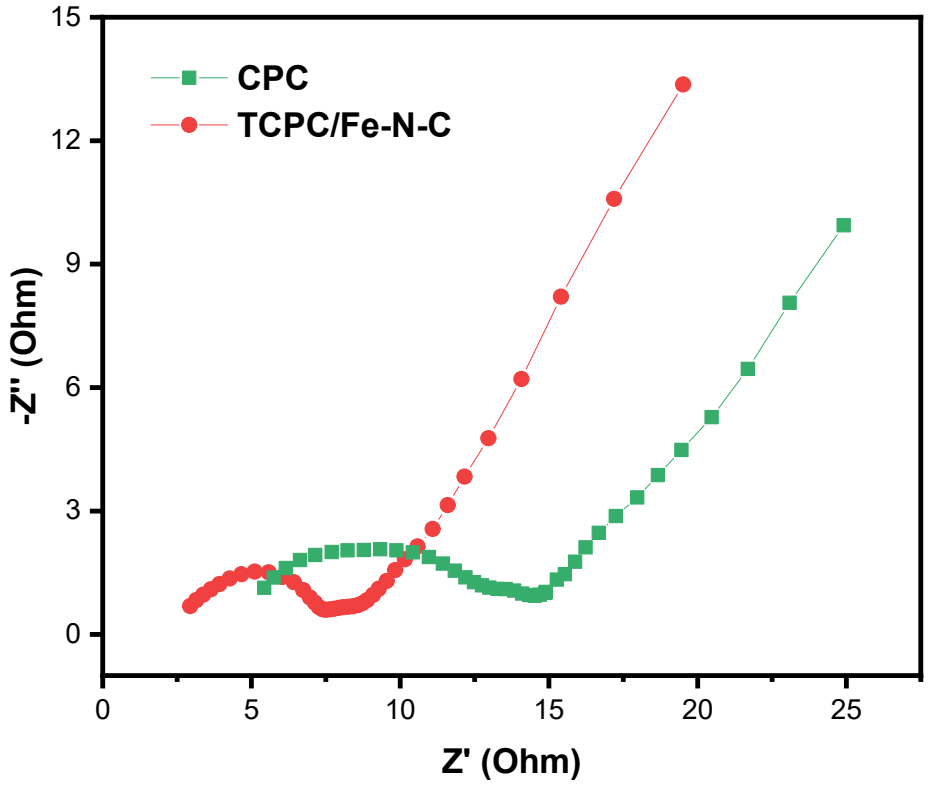

Fig. S34 EIS analysis data of CPC and TCPC/Fe-N-C after 50 charging and discharging at 2.0 C current density.

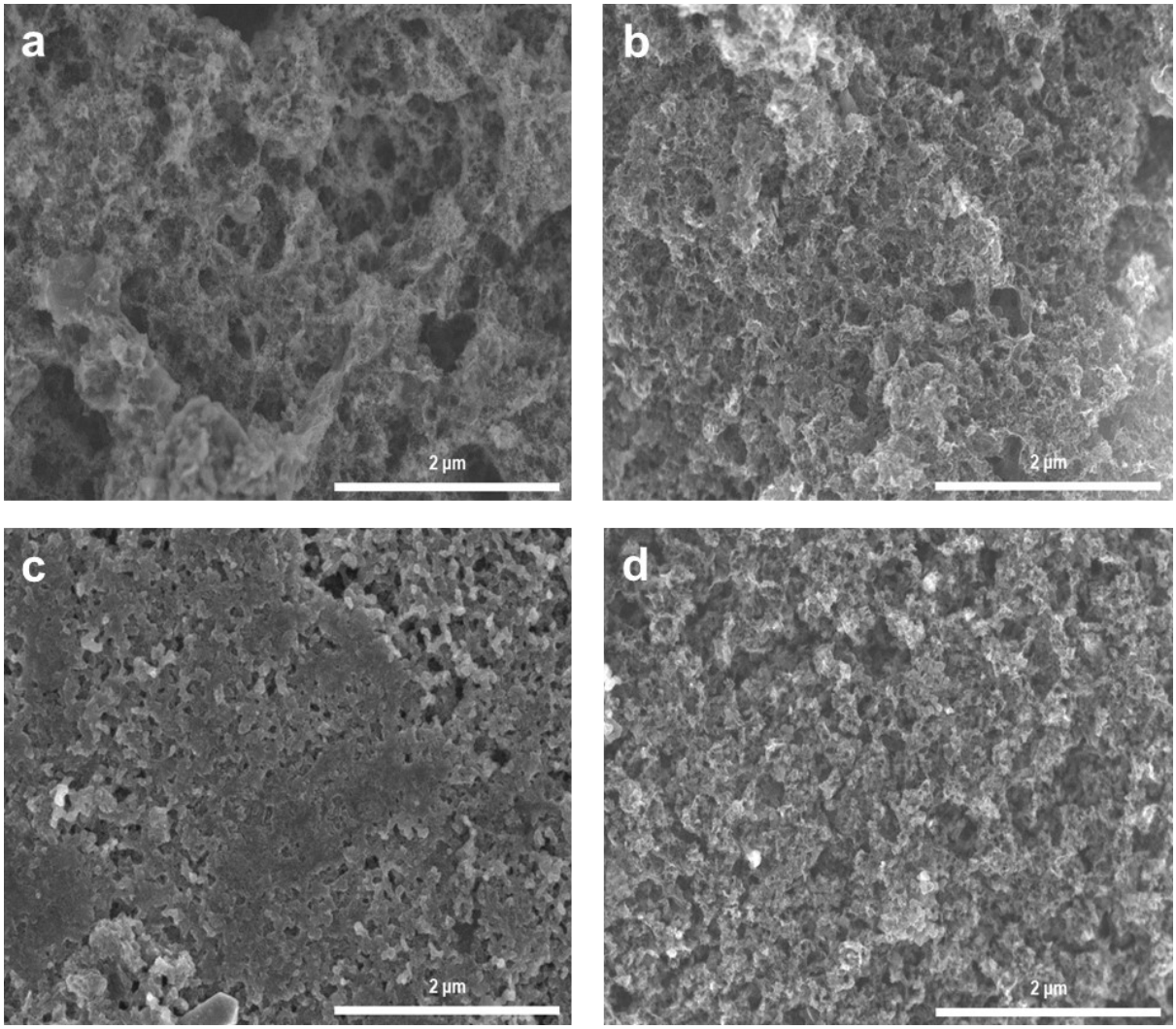

Fig. S35 SEM images of sulfur impregnated a) CPC, b) TCPC/Fe-N-C. SEM image of electrode surface of c) CPC, d) TCPC/Fe-N-C operated at 2.0 C for 50 cycles.

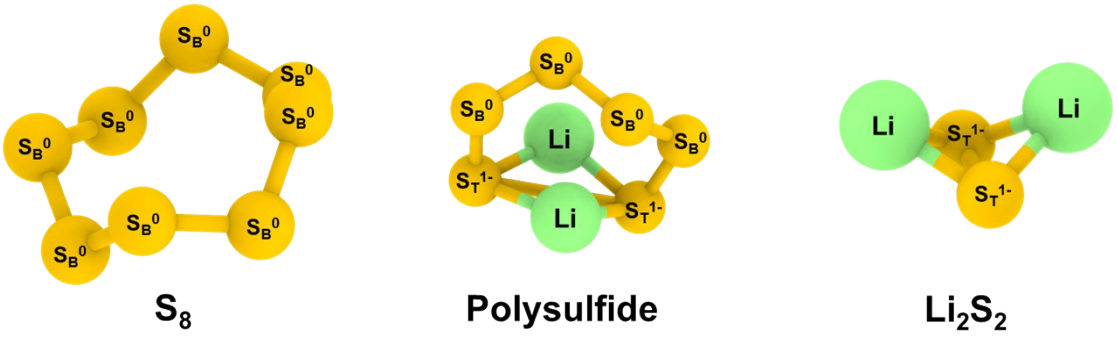

Fig. S36 3D schematic images of sulfur, polysulfide, and Li_2S_2 for XPS analysis.

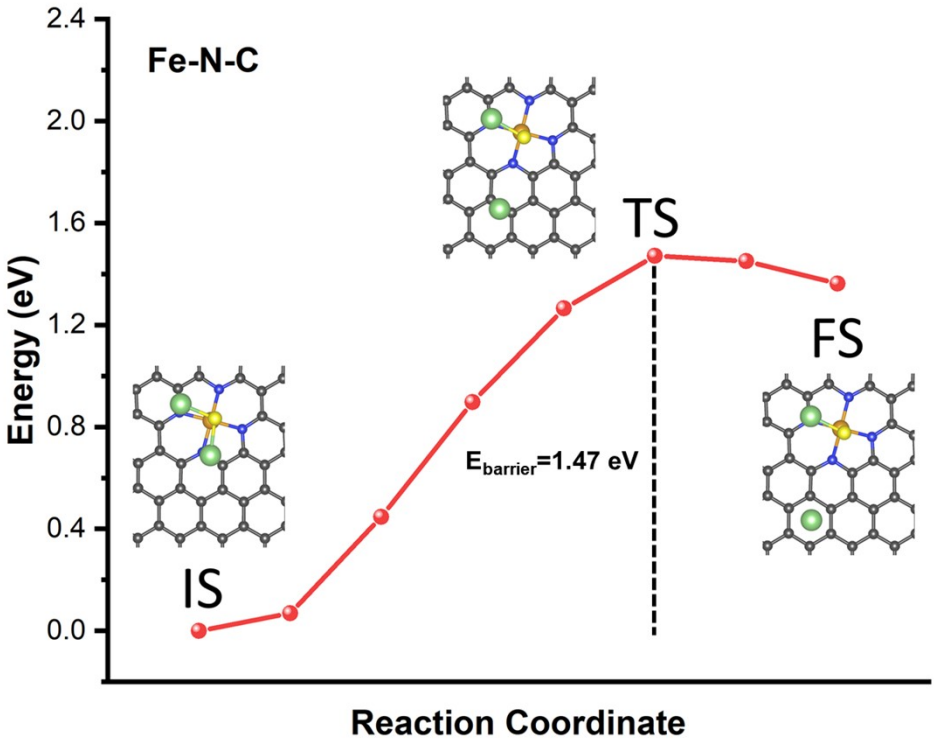

Fig. S37 Energy profiles and structural change in initial, transition, and final state when Li_2S is dissociated on Fe-N-C.

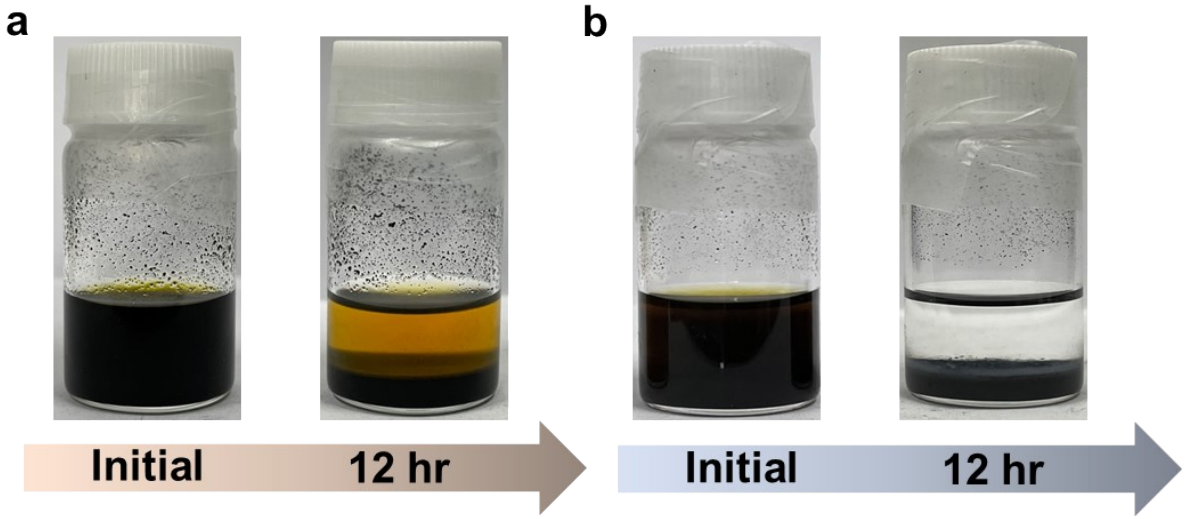

Fig. S38 Digital photographs of static adsorption test with a) CPC, b) TCPC/Fe-N-C powder.

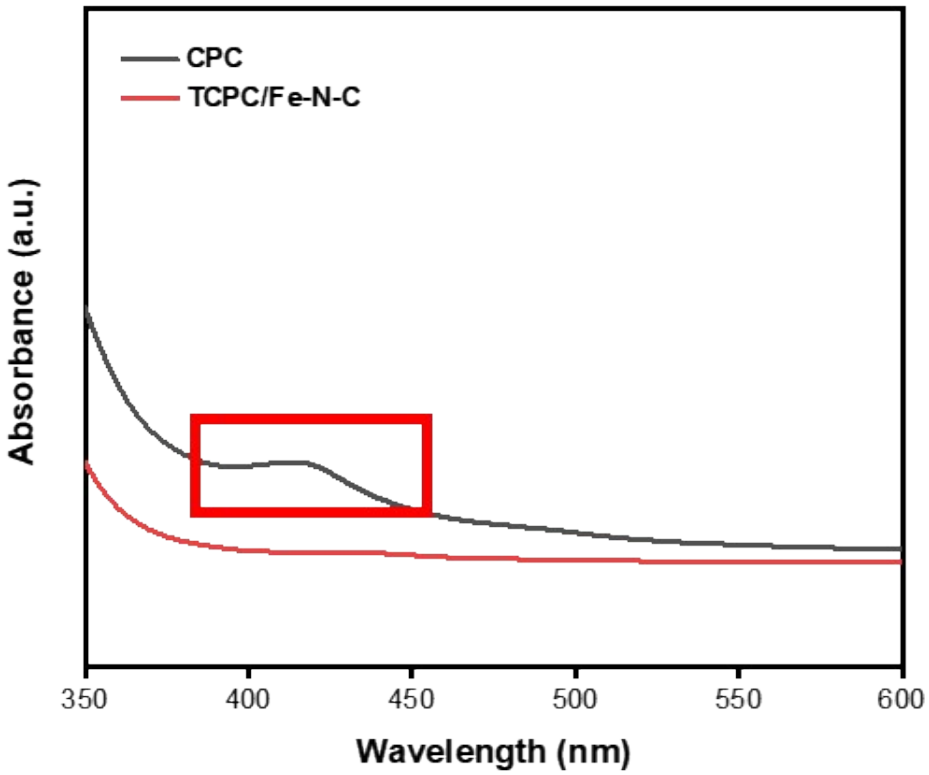

Fig. S39 UV−vis spectra of extracted solution after static adsorption test.

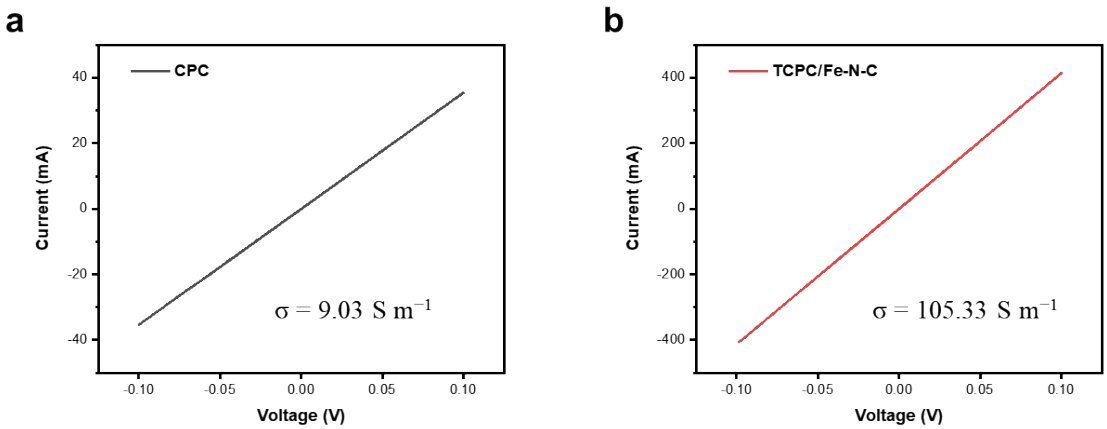

Fig. S40 I-V curve data obtained through a four-point probe method for the bulk conductivity (σ) of a) CPC, b) TCPC/Fe-N-C. (The diameter and thickness of pellets were unified to 1 cm and 2 mm, respectively.)

Table S1. The carbon, oxygen, and nitrogen content in CPC, UCPC/Fe-N-C, and TCPC/Fe-N-C samples by elemental analysis (EA).

Sample	CPC	UCPC/Fe-N-C	TCPC/Fe-N-C
Carbon content (wt%)	89.274	86.842	83.983
Oxygen content (wt%)	4.921	3.885	2.471
Nitrogen content (wt%)	0.079	1.392	4.391

Table S2. The BET measurement textual data of CPC, UCPC/Fe-N-C, and TCPC/Fe-N-C.

Sample	CPC	UCPC/Fe-N-C	TCPC/Fe-N-C
Specific surface area[A] (m^2 g^{-1})	1216	856	1049
Total pore volume[B] (cm^3 g^{-1})	3.355	2.902	3.364
Micro PV[C] (cm^3 g^{-1})	0.310	0.186	0.190
Meso PV[D] (cm^3 g^{-1})	3.045	2.716	3.174

[A]Brunauer-Emmett-Teller (BET) theory.
[B]Total pore volume up to P/P° of 0.99.
[C]Micropore volume was obtained by the NLDFT method.
[D]Mesopore volume was obtained by the NLDFT method.

Table S3. Surface atomic contents of XPS N1s spectra for UCPC/Fe-N-C and TCPC/Fe-N-C.

Atom	Bonding	Peak location	UCPC/Fe-N-C	TCPC/Fe-N-C
N1s	Pyridinic-N	398.5 eV	0.24 at%	1.30 at%
	Fe-N	399.4 eV	0.22 at%	0.78 at%
	Pyrrolic-N	400.4 eV	0.14 at%	1.17 at%
	Graphitic-N	401.7 eV	0.57 at%	0.90 at%
	Nitrite	404.0 eV	-	0.66 at%
	Nitrate	406.9 eV	0.36 at%	0.47 at%
N total			1.53 at%	5.28 at%

Table S4. Structural parameters for Fe foil, UCPC/Fe-N-C and TCPC/Fe-N-C secured through EXAFS fit based on the IFEFFIT code.

Sample	Pair	Coordination Number	Bond length (Å)	σ^2 (*10^{-3} Å^2)	R factor
Fe foil	Fe-Fe	8	2.46	6.26	0.006
		6	2.84	4.89	
UCPC/Fe-N-C	Fe-N	3.4	1.99	7.18	0.019
TCPC/Fe-N-C	Fe-N	3.6	1.99	7.62	0.017

σ^2 means Debye-waller factor, which is related to thermal and static disorders, and the amplitude reduction factor (S_o^2) was secured through the reference Fe foil and its value was set to 0.81.

Table S5. Calculated adsorption energy of lithium sulfides for bare graphene and Fe-N-C active sites.

	Li_2S	Li_2S_2	Li_2S_4	Li_2S_6	Li_2S_8
Graphene	−1.37303 eV	−1.41691 eV	−1.26386 eV	−1.45226 eV	−1.58662 eV
Fe-N-C	−2.73787 eV	−2.42183 eV	−1.93694 eV	−1.86123 eV	−2.13758 eV

Table S6. The comparison of BET characteristics, catalyst amount, and areal capacity with other studies using iron-based catalyst.

Sample	Surface area	Pore volume	Fe-based catalyst amount	Areal sulfur density	Current density	Cycle	Areal capacity
TCPC/Fe-N-C	1049 $m^2 g^{-1}$	3.364 $cm^3 g^{-1}$	0.45 wt%	4.3 mg cm^{-2}	1.0 C	300	2.11 mAh cm^{-2}
YSC@Fe_3O_4[1]	245 $m^2 g^{-1}$	0.9 $cm^3 g^{-1}$	21 wt%	5.5 mg cm^{-2}	0.1 C	200	4.7 mAh cm^{-2}
Fe-PNC[2]	240 $m^2 g^{-1}$	0.76 $cm^3 g^{-1}$	-	1.3 mg cm^{-2}	0.5 C	300	0.72 mAh cm^{-2}
[A]Fe_3C/Fe-N_x@NPCN[3]	266 $m^2 g^{-1}$	-	-	5.0 mg cm^{-2}	0.1 C	200	2.98 mAh cm^{-2}
Fe/N-HPCNF[4]	487 $m^2 g^{-1}$	-	2.88 wt%	3.5 mg cm^{-2}	0.5 C	500	3.00 mAh cm^{-2}
[A]Fe_3C-N-rGO[5]	251 $m^2 g^{-1}$	1.392 $cm^3 g^{-1}$	-	0.7 mg cm^{-2}	0.5 C	100	0.51 mAh cm^{-2}
Fe_3O_4@CNTs nanospheres[6]	164 $m^2 g^{-1}$	-	23 wt%	5.5 mg cm^{-2}	1.0 C	100	2.85 mAh cm^{-2}
[A]Fe_3C/C membrane[7]	6.618 $m^2 g^{-1}$	-	8.5 wt%	3.4 mg cm^{-2}	1.0 C	200	2.04 mAh cm^{-2}
[A]Fe-N-C/G[8]	463 $m^2 g^{-1}$	0.316 $cm^3 g^{-1}$	-	1.0 mg cm^{-2}	0.5 C	500	0.60 mAh cm^{-2}
HFeNG[9]	371 $m^2 g^{-1}$	-	-	5.0 mg cm^{-2}	0.1 C	100	3.00 mAh cm^{-2}
Fe-N-C/S-MCF[10]	-	-	0.33 wt%	5.2 mg cm^{-2}	3.0 C	500	2.00 mAh cm^{-2}
[A]Fe_3O_4/CNSs-PP[11]	799 $m^2 g^{-1}$	0.41 $cm^3 g^{-1}$	43. 6 wt%	4.7 mg cm^{-2}	1.0 C	100	2. 67 mAh cm^{-2}
GFS-15[12]	374 $m^2 g^{-1}$	1.45 $cm^3 g^{-1}$	15 wt%	2.6 mg cm^{-2}	1.0 C	600	1.19 mAh cm^{-2}
[A]Fe_3C/CNF interlayer[13]	62 $m^2 g^{-1}$	-	-	2.3 mg cm^{-2}	0.12 C	100	2.05 mAh cm^{-2}
CI-2-Tef[14]	3105 $m^2 g^{-1}$	3.32 $cm^3 g^{-1}$	3 wt%	1.8 mg cm^{-2}	0.2 C	500	1.98 mAh cm^{-2}
[A]Fe_3O_4@C/CNTO[15]			5.4 wt%		1.0 C	300	1.10 mAh cm^{-2}
Fe_3O_4/NC/G[16]	266 $m^2 g^{-1}$	0.36 $cm^3 g^{-1}$	41.5 wt%	7.7 mg cm^{-2}	0.5 C	100	5.67 mAh cm^{-2}
Fe_2N@C NBs[17]	201 $m^2 g^{-1}$	-	40 wt%	4.1 mg cm^{-2}	0.5 C	100	3.49 mAh cm^{-2}
[A]Fe@NG/PP[18]				1.1 mg cm^{-2}	2.0 C	200	0.546 mAh cm^{-2}

[A]Sample was used as Interlayer.

Reference

1. J. He, L. Luo, Y. Chen and A. Manthiram, *Adv. Mater.*, 2017, **29**, 1702707.
2. Z. Liu, L. Zhou, Q. Ge, R. Chen, M. Ni, W. Utetiwabo, X. Zhang and W. Yang, *ACS Appl. Mater. Interfaces*, 2018, **10**, 19311-19317.
3. H. Yang, Y. Yang, X. Zhang, Y. Li, N. A. Qaisrani, F. Zhang and C. Hao, *ACS Appl. Mater. Interfaces*, 2019, **11**, 31860-31868.
4. M. Jiang, R. Wang, K. Wang, S. Gao, J. Han, J. Yan, S. Cheng and K. Jiang, *Nanoscale*, 2019, **11**, 15156-15165.
5. H. Pan, Z. Tan, H. Zhou, L. Jiang, Z. Huang, Q. Feng, Q. Zhou, S. Ma and Y. Kuang, *J. Energy Chem.*, 2019, **39**, 101-108.
6. Y. Zhang, R. Gu, S. Zheng, K. Liao, P. Shi, J. Fan, Q. Xu and Y. Min, *J. Mater. Chem. A*, 2019, **7**, 21747-21758.
7. W. Kou, G. Chen, Y. Liu, W. Guan, X. Li, N. Zhang and G. He, *J. Mater. Chem. A*, 2019, **7**, 20614-20623.
8. X. Song, S. Wang, G. Chen, T. Gao, Y. Bao, L.-X. Ding and H. Wang, *Chem. Eng. J.*, 2018, **333**, 564-571.
9. Y. Wang, D. Adekoya, J. Sun, T. Tang, H. Qiu, L. Xu, S. Zhang and Y. Hou, *Adv. Funct. Mater.*, 2019, **29**, 1807485.
10. W.-G. Lim, Y. Mun, A. Cho, C. Jo, S. Lee, J. W. Han and J. Lee, *ACS Nano*, 2018, **12**, 6013-6022.
11. Z. Su, M. Chen, Y. Pan, Y. Liu, H. Xu, Y. Zhang and D. Long, *J. Mater. Chem. A*, 2020, **8**, 24117-24127.
12. H. Zhang, Q. Gao, X. Tian, Z. Li, P. Xu and H. Xiao, *Electrochim. Acta*, 2019, **319**, 472-480.
13. J.-Q. Huang, B. Zhang, Z.-L. Xu, S. Abouali, M. Akbari Garakani, J. Huang and J.-K. Kim, *J. Power Sources*, 2015, **285**, 43-50.
14. H. Wei, E. F. Rodriguez, A. S. Best, A. F. Hollenkamp, D. Chen and R. A. Caruso, *ACS Appl. Mater. Interfaces*, 2019, **11**, 13194-13204.
15. J. Du, W. Ahmed, J. Xu, M. Zhang, Z. Zhang, X. Zhang and D. Niu, *ChemistrySelect*, 2020, **5**, 3757-3762.
16. M. Ding, S. Huang, Y. Wang, J. Hu, M. E. Pam, S. Fan, Y. Shi, Q. Ge and H. Y. Yang, *J. Mater. Chem. A*, 2019, **7**, 25078-25087.
17. W. Sun, C. Liu, Y. Li, S. Luo, S. Liu, X. Hong, K. Xie, Y. Liu, X. Tan and C. Zheng, *ACS Nano*, 2019, **13**, 12137-12147.
18. G. Cao, Z. Wang, D. Bi, J. Zheng, Q. Lai and Y. Liang, *Chemistry*, 2020, **26**, 10314-10320.